7. Imai Y, Soda M, Takahashi R: **Parkin suppresses unfolded protein stress-induced cell death through its E3 ubiquitin-protein ligase activity.** *J Biol Chem* 2000, **275**:35661-35664.

8. Shimura H, Hattori N, Kubo S, Mizuno Y, Asakawa S, Minoshima S, Shimizu N, Iwai K, Chiba T, Tanaka K *et al.*: **Familial Parkinson disease gene product, Parkin, is a ubiquitin-protein ligase.** *Nat Genet* 2000, **25**:302-305.

9. Zhang Y, Gao J, Chung KK, Huang H, Dawson VL, Dawson TM: **Parkin functions as an E2-dependent ubiquitin- protein ligase and promotes the degradation of the synaptic vesicle-associated protein, CDCrel-1.** *Proc Natl Acad Sci USA* 2000, **97**:13354-13359.

10. Staropoli JF, McDermott C, Martinat C, Schulman B, Demireva E, Abeliovich A: **Parkin is a component of an SCF-like ubiquitin ligase complex and protects postmitotic neurons from kainate excitotoxicity.** *Neuron* 2003, **37**:735-749.

11. Imai Y, Soda M, Hatakeyama S, Akagi T, Hashikawa T, Nakayama KI, Takahashi R: **CHIP is associated with Parkin, a gene responsible for familial Parkinson's disease, and enhances its ubiquitin ligase activity.** *Mol Cell* 2002, **10**:55-67.

12. Tsai YC, Fishman PS, Thakor NV, Oyler GA: **Parkin facilitates the elimination of expanded polyglutamine proteins and leads to preservation of proteasome function.** *J Biol Chem* 2003, **278**:22044-22055.

13. Murata S, Minami Y, Minami M, Chiba T, Tanaka K: **CHIP is a chaperone-dependent E3 ligase that ubiquitylates unfolded protein.** *EMBO Rep* 2001, **2**:1133-1138.

14. Peng XR, Jia Z, Zhang Y, Ware J, Trimble WS: **The septin CDCrel-1 is dispensable for normal development and neurotransmitter release.** *Mol Cell Biol* 2002, **22**:378-387.

15. • Dong Z, Ferger B, Paterna JC, Vogel D, Furler S, Osinde M, Feldon J, Bueler H: **Dopamine-dependent neurodegeneration in rats induced by viral vector-mediated overexpression of the Parkin target protein, CDCrel-1.** *Proc Natl Acad Sci USA* 2003, **100**:12438-12443.

This *in vivo* study using a recombinant adeno-associated virus shows that CDCrel-1 over-expression in nigrostriatal regions induces selective degeneration of TH-positive neurons, which can be prevented by inhibition of dopamine synthesis.

16. • Yang Y, Nishimura I, Imai Y, Takahashi R, Lu B: **Parkin suppresses dopaminergic neuron-selective neurotoxicity induced by Pael-R in *Drosophila*.** *Neuron* 2003, **37**:911-924.

The authors demonstrate that Pael-R overexpression in the fly brain results in the elimination of TH-positive neurons but not other neurons, which is enhanced by Parkin knockdown using RNA interference. This result, together with that of Dong *et al.* [15•], suggests that a common mechanism underlies the degeneration of TH-positive neurons by over-expression of CDCrel-1 or Pael-R, and that dopamine and dopamine metabolites are involved in this process. They also show that Parkin overexpression suppresses α-synuclein neurotoxicity in the fly brain.

17. Murakami T, Shoji M, Imai Y, Inoue H, Kawarabayashi T, Matsubara E, Harigaya Y, Sasaki A, Takahashi R, Abe K: **Pael-R is accumulated in Lewy bodies of Parkinson's disease.** *Ann Neurol* 2004, **55**:439-442.

18. Corti O, Hampe C, Koutnikova H, Darios F, Jacquier S, Prigent A, Robinson JC, Pradier L, Ruberg M, Mirande M *et al.*: **The p38 subunit of the aminoacyl-tRNA synthetase complex is a Parkin substrate: linking protein biosynthesis and neurodegeneration.** *Hum Mol Genet* 2003, **12**:1427-1437.

19. Huynh DP, Scoles DR, Nguyen D, Pulst SM: **The autosomal recessive juvenile Parkinson disease gene product, Parkin, interacts with and ubiquitinates synaptotagmin XI.** *Hum Mol Genet* 2003, **12**:2587-2597.

20. Petrucelli L, O'Farrell C, Lockhart PJ, Baptista M, Kehoe K, Vink L, Choi P, Wolozin B, Farrer M, Hardy J *et al.*: **Parkin protects against the toxicity associated with mutant alpha-synuclein: proteasome dysfunction selectively affects catecholaminergic neurons.** *Neuron* 2002, **36**:1007-1019.

21. Oluwatosin-Chigbu Y, Robbins A, Scott CW, Arriza JL, Reid JD, Zysk JR: **Parkin suppresses wild-type alpha-synuclein-induced toxicity in SHSY-5Y cells.** *Biochem Biophys Res Commun* 2003, **309**:679-684.

22. • Winklhofer KF, Henn IH, Kay-Jackson PC, Heller U, Tatzelt J: **Inactivation of Parkin by oxidative stress and C-terminal truncations: a protective role of molecular chaperones.** *J Biol Chem* 2003, **278**:47199-47208.

This study suggests the possibility that oxidative stress inactivates Parkin. Treatment of Parkin-expressing cells with thermal and oxidative stress promotes the formation of 0.1% triton X-100-insoluble Parkin protein, a phenomenon that is suppressed by the induction of heat shock chaperones.

23. Hyun DH, Lee M, Hattori N, Kubo S, Mizuno Y, Halliwell B, Jenner P: **Effect of wild-type or mutant Parkin on oxidative damage, nitric oxide, antioxidant defences, and the proteasome.** *J Biol Chem* 2002, **277**:28572-28577.

24. Darios F, Corti O, Lucking CB, Hampe C, Muriel MP, Abbas N, Gu WJ, Hirsch EC, Rooney T, Ruberg M *et al.*: **Parkin prevents mitochondrial swelling and cytochrome c release in mitochondria-dependent cell death.** *Hum Mol Genet* 2003, **12**:517-526.

25. • Greene JC, Whitworth AJ, Kuo I, Andrews LA, Feany MB, Pallanck LJ: **Mitochondrial pathology and apoptotic muscle degeneration in *Drosophila parkin* mutants.** *Proc Natl Acad Sci USA* 2003, **100**:4078-4083.

This is the first report of a Parkin-deficient animal. The authors created several lines of *Drosophila parkin* null mutants so these mutants exhibit a more severe phenotype caused by mitochondria dysfunction rather than pathology of AR-JP. However, degeneration of TH-positive neurons was not observed.

26. • Sakata E, Yamaguchi Y, Kurimoto E, Kikuchi J, Yokoyama S, Yamada S, Kawahara H, Yokosawa H, Hattori N, Mizuno Y *et al.*: **Parkin binds the Rpn10 subunit of 26S proteasomes through its ubiquitin-like domain.** *EMBO Rep* 2003, **4**:301-306.

This structural study, together with the nuclear magnetic resonance (NMR) study of Tashiro *et al.* [27], reveals that the Ubl of Parkin has a typical ubiquitin fold. This study also shows that the arginine residue at amino-acid position 42 within the Ubl, where an AR-JP-related single mutation (R42P) has been found, contributes to the interaction with a subunit of the 26S proteasome, which provides strong evidence for the involvement of Parkin in protein breakdown.

27. Tashiro M, Okubo S, Shimotakahara S, Hatanaka H, Yasuda H, Kainosho M, Yokoyama S, Shindo H: **NMR structure of ubiquitin-like domain in Parkin: gene product of familial Parkinson's disease.** *J Biomol NMR* 2003, **25**:153-156.

28. Upadhya SC, Hegde AN: **A potential proteasome-interacting motif within the ubiquitin-like domain of Parkin and other proteins.** *Trends Biochem Sci* 2003, **28**:280-283.

29. Finney N, Walther F, Mantel PY, Stauffer D, Rovelli G, Dev KK: **The cellular protein level of Parkin is regulated by its ubiquitin-like domain.** *J Biol Chem* 2003, **278**:16054-16058.

30. Pawlyk AC, Giasson BI, Sampathu DM, Perez FA, Lim KL, Dawson VL, Dawson TM, Palmiter RD, Trojanowski JQ, Lee VM: **Novel monoclonal antibodies demonstrate biochemical variation of brain Parkin with age.** *J Biol Chem* 2003, **278**:48120-48128.

31. Schlossmacher MG, Frosch MP, Gai WP, Medina M, Sharma N, Forno L, Ochiishi T, Shimura H, Sharon R, Hattori N *et al.*: **Parkin localizes to the Lewy bodies of Parkinson's disease and dementia with Lewy bodies.** *Am J Pathol* 2002, **160**:1655-1667.

32. Muqit MM, Davidson SM, Payne Smith MD, MacCormac LP, Kahns S, Jensen PH, Wood NW, Latchman DS: **Parkin is recruited into aggresomes in a stress-specific manner: over-expression of Parkin reduces aggresome formation but can be dissociated from Parkin's effect on neuronal survival.** *Hum Mol Genet* 2004, **13**:117-135.

33. Kahns S, Lykkebo S, Jakobsen LD, Nielsen MS, Jensen PH: **Caspase-mediated Parkin cleavage in apoptotic cell death.** *J Biol Chem* 2002, **277**:15303-15308.

34. Kahns S, Kalai M, Jakobsen LD, Clark BF, Vandenabeele P, Jensen PH: **Caspase-1 and caspase-8 cleave and inactivate cellular Parkin.** *J Biol Chem* 2003, **278**:23376-23380.

35. Mengesdorf T, Jensen PH, Mies G, Aufenberg C, Paschen W: **Down-regulation of Parkin protein in transient focal cerebral ischemia: a link between stroke and degenerative disease?** *Proc Natl Acad Sci USA* 2002, **99**:15042-15047.

36. West AB, Gonzalez-de-Chavez F, Wilkes K, O'Farrell C, Farrer MJ: **Parkin is not regulated by the unfolded protein response in human neuroblastoma cells.** *Neurosci Lett* 2003, **341**:139-142.

37. Ledesma MD, Galvan C, Hellias B, Dotti C, Jensen PH: **Astrocytic but not neuronal increased expression and redistribution of Parkin during unfolded protein stress.** *J Neurochem* 2002, **83**:1431-1440.

38. Ardley HC, Scott GB, Rose SA, Tan NG, Markham AF, Robinson PA: **Inhibition of proteasomal activity causes inclusion formation in neuronal and non-neuronal cells overexpressing Parkin.** *Mol Biol Cell* 2003, **14**:4541-4556.

39. • Junn E, Lee SS, Suhr UT, Mouradian MM: **Parkin accumulation in aggresomes due to proteasome impairment.** *J Biol Chem* 2002, **277**:47870-47877.
This *in vitro* study of the effects of proteasome inhibitors shows that Parkin, as well as α-synuclein and other proteins within LBs, co-localizes within aggresomes in cultured cells. This result implies that aggresome formation is related to that of LBs in PD. The studies of Ardley *et al.* [38], Zhao *et al.* [40] and Imai *et al.* [41] give similar results.

40. Zhao J, Ren Y, Jiang Q, Feng J: **Parkin is recruited to the centrosome in response to inhibition of proteasomes.** *J Cell Sci* 2003, **116**:4011-4019.

41. Imai Y, Soda M, Murakami T, Shoji M, Abe K, Takahashi R: **A product of the human gene adjacent to parkin is a component of Lewy bodies and suppresses Pael receptor-induced cell death.** *J Biol Chem* 2003, **278**:51901-51910.

42. •• Itier JM, Ibáñez P, Mena MA, Abbas N, Cohen-Salmon C, Bohme GA, Laville M, Pratt J, Corti O, Pradier L *et al.*: **Parkin gene inactivation alters behaviour and dopamine neurotransmission in the mouse.** *Hum Mol Genet* 2003, **12**:2277-2291.
This paper is the first report of Parkin-deficient mice, in which the authors observed pre-synaptic dysfunction of neurons, along with an increase in dopamine and dopamine metabolites, and motor and cognitive deficits. However, neither this nor a subsequent report by Goldberg *et al.* [43•] observed macroscopic degeneration of dopaminergic neurons with age.

43. • Goldberg MS, Fleming SM, Palacino JJ, Cepeda C, Lam HA, Bhatnagar A, Meloni EG, Wu N, Ackerson LC, Klapstein GJ *et al.*: **Parkin-deficient mice exhibit nigrostriatal deficits but not loss of dopaminergic neurons.** *J Biol Chem* 2003, **278**:43628-43635.
This study shows an increase in extracellular dopamine within the striatum by microdialysis. Electrophysiological deficits in striatal neurons and motor deficits in Parkin-deficient mice are also demonstrated.

44. Ihara M, Tomimoto H, Kitayama H, Morioka Y, Akiguchi I, Shibasaki H, Noda M, Kinoshita M: **Association of the cytoskeletal GTP-binding protein Sept4/H5 with cytoplasmic inclusions found in Parkinson's disease and other synucleinopathies.** *J Biol Chem* 2003, **278**:24095-24102.

45. Shimura H, Schlossmacher MG, Hattori N, Frosch MP, Trockenbacher A, Schneider R, Mizuno Y, Kosik KS, Selkoe DJ: **Ubiquitination of a new form of alpha-synuclein by Parkin from human brain: implications for Parkinson's disease.** *Science* 2001, **293**:263-269.

46. Imai Y, Soda M, Inoue H, Hattori N, Mizuno Y, Takahashi R: **An unfolded putative transmembrane polypeptide, which can lead to endoplasmic reticulum stress, is a substrate of Parkin.** *Cell* 2001, **105**:891-902.

47. Ren Y, Zhao J, Feng J: **Parkin binds to alpha/beta tubulin and increases their ubiquitination and degradation.** *J Neurosci* 2003, **23**:3316-3324.

48. Iseki E, Marui W, Sawada H, Ueda K, Kosaka K: **Accumulation of human alpha-synuclein in different cytoskeletons in Lewy bodies in brains of dementia with Lewy bodies.** *Neurosci Lett* 2000, **290**:41-44.

49. Chung KK, Zhang Y, Lim KL, Tanaka Y, Huang H, Gao J, Ross CA, Dawson VL, Dawson TM: **Parkin ubiquitinates the alpha-synuclein-interacting protein, synphilin- 1: implications for Lewy-body formation in Parkinson's disease.** *Nat Med* 2001, **7**:1144-1150.

50. Wakabayashi K, Engelender S, Yoshimoto M, Tsuji S, Ross CA, Takahashi H: **Synphilin-1 is present in Lewy bodies in Parkinson's disease.** *Ann Neurol* 2000, **47**:521-523.

51. Choi P, Snyder H, Petrucelli L, Theisler C, Chong M, Zhang Y, Lim K, Chung KK, Kehoe K, D'Adamio L *et al.*: **SEPT5_v2 is a parkin-binding protein.** *Brain Res Mol Brain Res* 2003, **117**:179-189.

Superoxide Production at Phagosomal Cup/Phagosome through βI Protein Kinase C during FcγR-Mediated Phagocytosis in Microglia[1]

Takehiko Ueyama,* Michelle R. Lennartz,*† Yukiko Noda,‡ Toshihiro Kobayashi,§ Yasuhito Shirai,* Kyoko Rikitake,* Tomoko Yamasaki,‡ Shigeto Hayashi,* Norio Sakai,*¶ Harumichi Seguchi,§ Makoto Sawada,‖ Hideki Sumimoto,## and Naoaki Saito[2]*

Protein kinase C (PKC) plays a prominent role in immune signaling. To elucidate the signal transduction in a respiratory burst and isoform-specific function of PKC during FcγR-mediated phagocytosis, we used live, digital fluorescence imaging of mouse microglial cells expressing GFP-tagged molecules. βI PKC, εPKC, and diacylglycerol kinase (DGK) β dynamically and transiently accumulated around IgG-opsonized beads (BIgG). Moreover, the accumulation of $p47^{phox}$, an essential cytosolic component of NADPH oxidase and a substrate for βI PKC, at the phagosomal cup/phagosome was apparent during BIgG ingestion. Superoxide (O_2^-) production was profoundly inhibited by Gö6976, a cPKC inhibitor, and dramatically increased by the DGK inhibitor, R59949. Ultrastructural analysis revealed that BIgG induced O_2^- production at the phagosome but not at the intracellular granules. We conclude that activation/accumulation of βI PKC is involved in O_2^- production, and that O_2^- production is primarily initiated at the phagosomal cup/phagosome. This study also suggests that DGKβ plays a prominent role in regulation of O_2^- production during FcγR-mediated phagocytosis. *The Journal of Immunology,* **2004, 173: 4582–4589.**

Microglia have been described as resident macrophages in the CNS. Invading pathogens are removed via phagocytosis using the Fcγ, complement, scavenger, mannose, phosphatidylserine, and TLR (1). Over the past few years, phagocytosis in microglia, especially FcγR-mediated phagocytosis, has attracted a great deal of attention in the context of potential therapy for Alzheimer's disease (2).

Protein kinase C (PKC)[3] comprises a family of 10 isoforms (3). The conventional isoforms (cPKC; α, βI, βII, and γ) are Ca^{2+} and diacylglycerol (DAG)-dependent, the novel isoforms (nPKC; δ, ε, η, and θ) are also DAG-dependent, but Ca^{2+} independent, and the atypical isoforms (ζ and ιλ) are nonresponsive to Ca^{2+} or DAG. Phenotypes for various PKC knockout mice have shown a role for a specific isoform in the immune system. Mice deficient in βPKC have a marked immunodeficiency (4), and show a reduced production of the superoxide (O_2^-), a precursor of microbicidal oxidants, during FcγR-mediated phagocytosis in neutrophils *(5)*. In the absence of εPKC, host defense against bacterial infection is severely compromised (6). The signaling capacity of DAG can be terminated by its conversion to phosphatidic acid through the action of diacylglycerol kinase (DGK). DGK family is composed of nine mammalian subtypes and is grouped into five classes; type I DGK (α, β, and γ) has Ca^{2+}-binding motifs (7). Because excessive O_2^- production appears to be harmful to normal cells and tissues (8), it is implicated that O_2^- production involved in βPKC has a tight regulation by DGK isoform.

FcγR-mediated phagocytosis is a spatiotemporally regulated signaling cascade with two rapid responses, remodeling of the cytoskeleton and activation of the respiratory burst. Phospholipase C (PLC) γ, a key enzyme for actin remodeling, is activated upon engagement of FcγRs (9). DAG and inositol-1,4,5-triphosphate (IP_3) from PLCγ activation exert their effects by stimulating PKC or by changing intracellular Ca^{2+} concentration ($[Ca^{2+}]_i$), respectively. The respiratory burst is initiated by the phagocyte NADPH oxidase, which is dormant in resting cells, but becomes activated during phagocytosis to produce O_2^- (10). NADPH oxidase is a multiprotein complex that is assembled from a membrane-spanning cytochrome b_{558} ($gp91^{phox}$ and $p22^{phox}$) and four main cytosolic factors ($p47^{phox}$, $p67^{phox}$, $p40^{phox}$, and Rac) that translocate to the cytochrome b_{558} to generate the active enzyme. Various protein kinases, including PKC, MAPK, PKA, the p21-activated kinases, phosphatidic acid-regulated protein kinases, and Akt (protein kinase B) have been reported to activate NADPH oxidase through phosphorylation of $p47^{phox}$ (11, 12). In neutrophils stimulated by PMA, the intracellular granules are proposed as the initial O_2^--producing sites, then these granules fuse with the plasma

*Laboratory of Molecular Pharmacology, Biosignal Research Center, Kobe University, Kobe, Japan; †Center for Cell Biology and Cancer Research, Albany Medical College, Albany, NY 12208; §Department of Anatomy and Cell Biology, Kochi Medical School, Kochi, Japan; ‡Medical Institute of Bioregulation, Kyushu University, Fukuoka, Japan; ¶Graduate School of Biomedical Sciences, Hiroshima University, Hiroshima, Japan; ‖Institute for Comprehensive Medical Science, Fujita Health University, Toyoake, Japan; and ##CREST JST (Japan Science and Technology)

Received for publication April 5, 2004. Accepted for publication July 16, 2004.

The costs of publication of this article were defrayed in part by the payment of page charges. This article must therefore be hereby marked *advertisement* in accordance with 18 U.S.C. Section 1734 solely to indicate this fact.

[1] This work was supported by grants from the 21st Century Center of Excellence Program of the Ministry of Education, Culture, Sports, Science, and Technology of Japan, Core Research for Evolutional Science and Technology, the Ministry of Education, Culture, Sports, Science, and Technology in Japan, a Grant-in-Aid for Scientific Research on Priority Areas (C)-Advanced Brain Science Project from the Ministry of Education, Culture, Sports, Science, and Technology in Japan, the Uehara Memorial Foundation, and the Sankyo Foundation of Life Science.

[2] Address correspondence and reprint requests to Dr. Naoaki Saito, Laboratory of Molecular Pharmacology, Biosignal Research Center, Kobe University, Rokkodai-cho 1-1, Nada-ku, Kobe 657-8501, Japan. E-mail address: naosaito@kobe-u.ac.jp

[3] Abbreviations used in this paper: PKC, protein kinase C; DGK, diacylglycerol kinase; MARCKS, myristoylated alanine-rich C kinase substrate; c, conventional isoform; n, novel isoform; DAG, diacylglycerol; O_2^- superoxide; PLC, phospholipase C; IP_3, inositol-1,4,5-triphosphate; $[Ca^{2+}]_i$, intracellular Ca^{2+} concentration; BIgG, IgG-opsonized beads.

0022-1767/04/$02.00

membrane, resulting in the delivery of O_2^- into the extracellular milieu (13, 14). However, PMA is a nonphysiological stimulus and results obtained using PMA may not accurately reflect the cell response to a physiological stimulus.

We now face the challenge of defining 1) the PKC involved signal transduction pathway regulated by DGK, 2) the isoform-specific function of PKC, and 3) the intracellular site of O_2^- production, during a FcγR-mediated respiratory burst at the cellular level. Unfortunately, primary neutrophils have a severely limited lifetime ex vivo, and both primary and cultured neutrophils are difficult to be transfected. Monocytes have a markedly reduced capacity for O_2^- production compared with neutrophils. To overcome these problems, we used our microglial cells and visualized the accumulation of βI and εPKC, DGKβ and $p47^{phox}$ to the phagosome using real-time confocal laser scanning fluorescence microscopy. In this study, we show that βI PKC contributes to O_2^- production, and that DGKβ plays an important role in regulation of O_2^- production, probably in control of excessive O_2^- production. Finally, we demonstrate that the O_2^--producing site during FcγR-mediated phagocytosis is at the phagosomal cup/phagosome.

Materials and Methods

Reagents

Two-micrometer glass beads and carboxylated latex beads were obtained from Duke Scientific (Palo Alto, CA) and Polysciences (Warrington, PA), respectively. Eagle's MEM and endotoxin-free FBS were from Invitrogen Life Technologies (Carlsbad, CA). Bovine insulin and PMA were from Sigma-Aldrich (St. Louis, MO). Mouse GM-CSF was from Genzyme (Cambridge, MA). U73122 and U73343 were from Biomol (Plymouth Meeting, PA), and Gö6976 and R59949 were from Calbiochem (San Diego, CA). Fura 2-AM was from Dojindo (Kumamoto, Japan).

Cell culture

The 6-3 microglial cells are generated by spontaneous immortalization of primary microglia from *op/op* mice which are deficient of M-CSF-derived macrophages and severely monocytopenic (15, 16). The 6-3 cells closely resemble primary microglia with respect to microglia-specific gene expression and high migrating activity to the brain (15, 17). The 6-3 cells were maintained in Eagle's MEM supplemented with 10% endotoxin-free FBS, 5 μg/ml insulin, 0.2% glucose, and 0.2 ng/ml GM-CSF. For confocal imaging, Ca^{2+} measurements, phagocytosis assays, and ultrastructural studies, cells were seeded on 35-mm glass-bottom dishes (MatTek, Ashland, MA) without GM-CSF, and used after 48 h.

Construction of plasmids

The PKC-GFP (α, βI, βII, γ, δ, ε, η, and ζ) and GFP-DGK (α and γ) constructs were previously described (3, 18). Myristoylated alanine-rich C kinase substrate (MARCKS)-GFP and mutant MARCKS-GFP, whose all three putative PKC phosphorylation sites in the effector domain were substituted to Ala, were prepared as reported (19). DGKβ with the *Eco*RI site was produced by PCR, and was cloned into the *Eco*RI site in pEGFP-C1 (Clontech, Palo Alto, CA), and named as GFP-DGKβ. The C1 domain of δPKC (aa 159–280) with *Eco*RI/*Bgl*II sites was amplified by PCR, and was cloned into the *Eco*RI/*Bgl*II sites of BS 354 (19), and named as δPKC(C1)-GFP. The constructs encoding human $p47^{phox}$, $p67^{phox}$, and $p47^{phox}$(W193R) were previously described (20, 21). $p47^{phox}$ and $p47^{phox}$(W193R) was cloned into the *Bgl*II/*Eco*RI sites of pEGFP-C1, and named as GFP-$p47^{phox}$ and $p47^{phox}$(W193R), respectively.

Phagocytosis targets

IgG-opsonized glass beads (BIgG), fluorescently labeled BIgG, and control beads (BBSA) were prepared as described (3). Carboxylated latex beads were opsonized with IgG using the Carbodiimide kit (Polysciences).

Phagocytosis assay

The culture medium was replaced with $HBSS^{++}$ (3) and targets (50 per cell) were added. After incubation at 37°C for 20 min, cells were fixed with 4% PFA in 0.1 M phosphate buffer (pH 7.4). In inhibitor experiments, cells were preincubated in $HBSS^{++}$ containing the inhibitor. The number of completely engulfed targets per cell was counted in 50 cells using phase-contrast microscopy. The measurements were made in triplicate on at least three separate experiments, and results are presented as means ± SD.

Synchronized phagocytosis and cell fractionation

Synchronized phagocytosis and cell fractionation were performed as described with modifications (3, 22). The 6-3 cells in 10-cm dishes were treated with ice cold $HBSS^{++}$ (with or without inhibitor) containing BIgG (50 per cell). After 10 min on ice for target binding, the cells were warmed to 37°C for synchronized phagocytosis. At the indicated times, the cells were scraped and sonicated (3 × 10 s) in 400 μl of lysis buffer (18). The beads were allowed to settle 10 min on ice, and then the settled beads were sonicated again (2 × 10 s) to gain the phagosomal membrane. The beads were settled for 1 h, and the supernatant was centrifuged for 30 min at 100,000 × *g*. The pellet was solubilized in lysis buffer containing 1% Triton X-100. The samples were centrifuged again as above. The supernatant was designated as the membrane fraction containing the phagosomal membrane. After protein assay with bicinchoninic acid (Pierce, Rockford, IL), equal amounts of the membrane fraction (micrograms per lane) were subjected to SDS-PAGE and Western blotting (18).

Confocal imaging

The 6-3 cells were transfected using Superfect (Qiagen, Valencia, CA). After 24–30 h, the culture medium was replaced with 800 μl of $HBSS^{++}$, and cells were imaged using an LSM 510 invert (Carl Zeiss, Jena, Germany) confocal laser scanning fluorescence microscope with a heated stage and objective (×40 oil). Two hundred microliters of $HBSS^{++}$-containing targets (5 per cell) was added to each plate. To treat cells with inhibitor, the culture medium was replaced by a $HBSS^{++}$-containing inhibitor and preincubated for the indicated time. The images were collected at 3, 5, or 10 s intervals for 10 min. The time of addition of BIgG was chosen as time 0. In a 1-day experiment, >3 independent cell preparations (dishes) in each group were performed. In one dish, 1–3 cells which engulfed 1–5 BIgG for 10 min were selected for analysis in the study.

Ca^{2+} measurement

The 6-3 cells were loaded with 5 μM Fura 2-AM in HEPES buffer (18). After a 1-h incubation, the cells were resuspended in HEPES buffer. Fluorescence was monitored using the ARGUS/HiSCA system (Hamamatsu Photonics, Hamamatsu, Japan) using a dual wavelength excitation (340 and 380 nm) and at emission (510 nm). HEPES buffer containing targets (1 per cell) was added, and the images were collected at 1.5 s intervals for 5 min. In inhibitor experiments, cells were further incubated for the indicated time with HEPES buffer containing Fura 2-AM and the inhibitor. Cells were maintained at 37°C with a heated objective (×40 oil). Data are presented as the background-corrected 340:380 ratio of Fura 2 fluorescence.

O_2^- production assay

O_2^- production was determined as superoxide dismutase-inhibitable chemiluminescence (Diogenes; National Diagnostics, Atlanta, GA) as described previously (21). After the addition of the luminol-based substrate, the prewarmed cells (1.0×10^4) in $HBSS^{++}$ were stimulated with BIgG (1.0×10^6). The chemiluminescence was assayed for 20 min using a luminometer (Auto Lumat LB953; EG & G Berthold, Bad Wildbad, Germany).

In inhibitor experiments, cells were preincubated in an $HBSS^{++}$-containing inhibitor. The 6-3 cells incubated with stimulus in the absence of the inhibitor served as the positive control. Results are presented as the percent of the positive control (means ± SD).

Ultrastructural detection of an oxidant-producing site

The O_2^--producing site in 6-3 cells was detected using the cerium-based cytochemical method (23) with modifications (24). The reaction for the detection of H_2O_2 proceeds as follows: $NADPH + 2O_2 \rightarrow NADP^+ + H^+ + 2O_2^-$, $2O_2^- + 2H^+ \rightarrow H_2O_2 + O_2$, $H_2O_2 + CeCl_3 \rightarrow Ce(OH)_2OOH$, $Ce(OH)_3OOH$. The final cerous reaction products can be detected in the electron microscope as a precipitate. Treatment with the O_2^- scavenger, *p*-benzoquinone, causes complete abolishment of the reaction precipitate (24). The cells stimulated with either BIgG (latex, 5 per cells) or 1 μM PMA were incubated for 15 min at 37°C in HEPES buffer containing 1 mM $CeCl_3$, 1 mM NaN_3, and 20 mM tricine. NaN_3 was added to prevent the degradation of H_2O_2 by endogenous catalase. Tricine was used to protect Ce^{3+} in the reaction buffer from nonenzymatic precipitation. Exogenous NADPH and FAD are not necessary for the oxidant production in this method. The cells were fixed with 2% glutaraldehyde in HEPES buffer. After a cytochemical reaction, the cells were postfixed and then dehydrated and embedded in epoxy resin. Semithin sections (0.5 μm in thickness) were observed under a JEM-100S electron microscope (JEOL, Tokyo, Japan).

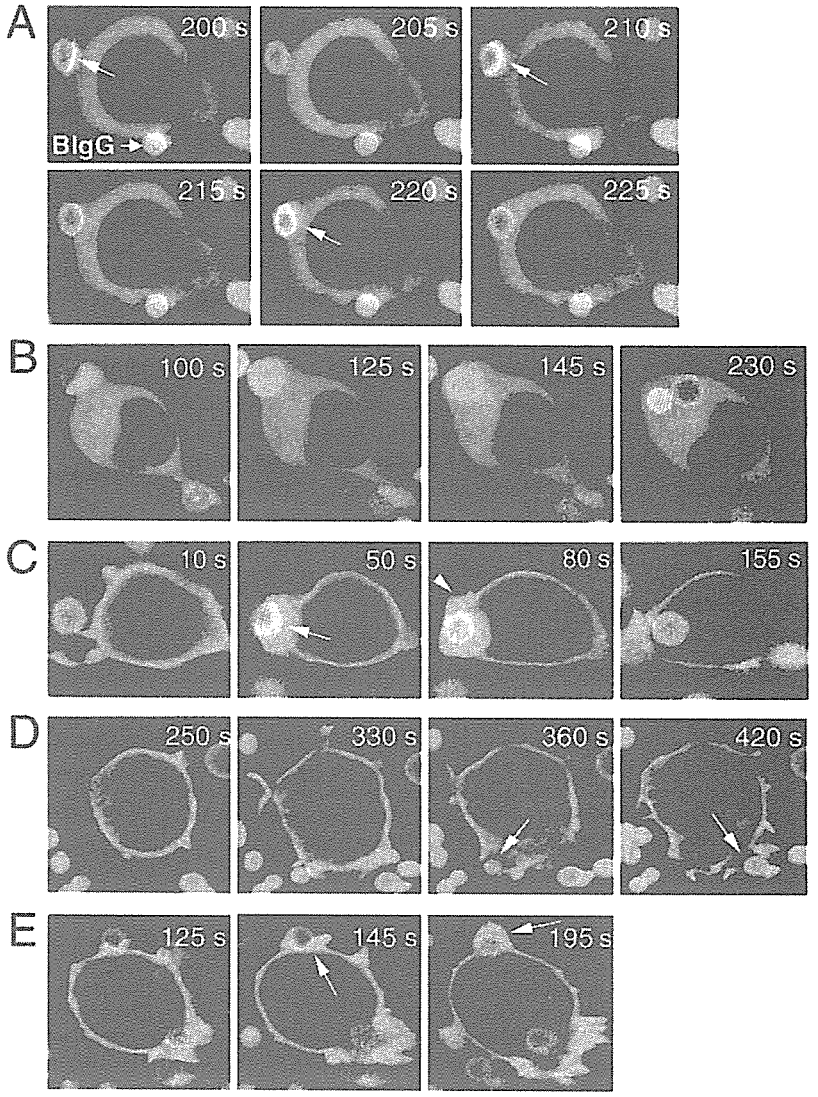

FIGURE 1. Accumulation of βI and εPKC, and DGKβ during FcγR-mediated phagocytosis. *A*, Oscillations in the accumulation of βI PKC-GFP at the phagosomal cup/phagosome is shown (arrows; cycle of oscillation is ~10 s; $n = >20$). No translocation of βI PKC-GFP to the plasma membrane is observed. A movie is available in Video 1. *B*, εPKC-GFP accumulates at the phagosomal cup/phagosome without oscillation ($n = >15$). *C*, GFP-DGKβ accumulates at the phagosomal cup (arrows) and at the plasma membrane (arrowhead), where BIgG was ingested. The accumulation was not apparent at the phagosome ($n = >20$). A movie is available in Video 2. *D*, MARCKS-GFP is released from the membrane of forming phagosome during internalization of BIgG (arrows; $n = >9$). *E*, The mutant MARCKS-GFP accumulated and was retained at the phagosomal cup and the forming phagosomal membrane (arrow) during internalization of BIgG.

Supporting information

The supplemental movies show the oscillatory accumulation of βI PKC-GFP (Video 1[4]) and the accumulation of DGKβ-GFP (Video 2) during phagocytosis of fluorescently labeled BIgG. Video 3 shows the oscillatory increase of $|Ca^{2+}|_i$ during phagocytosis of BIgG. Each movie represents >15 independent experiments.

Results

Characteristics of 6-3 microglial cells as phagocytes

We identified the PKC and type I DGK isoforms expressed in 6-3 microglial cells. Proteins of α, βI, δ, ε, η, and ζPKC and mRNAs for DGK α, β, and γ were detected by Western blotting and RT-PCR, respectively (data not shown); βII and γPKC were not detected in 6-3 cells. Expression of $gp91^{phox}$, $p22^{phox}$, $p47^{phox}$, $p67^{phox}$, and $p40^{phox}$ in 6-3 cells was confirmed by Western blotting; and expression of Rac1 and Rac2, but not Rac3, were confirmed by RT-PCR (data not shown). PMA-stimulated O_2^- production in 6-3 cells was about one-tenth of that observed in neutrophils (data not shown).

[4] The on-line version of this article contains supplemental material.

Isoform-specific accumulation of PKC-GFP and GFP-DGK in Fcγ-mediated phagocytosis

Of the six PKC isoforms (α, βI, δ, ε, η, and ζ PKC) expressed, only βI and εPKC-GFP showed the localized translocation to the phagosomal cup/phagosome during phagocytosis of BIgG in 6-3 cells (Fig. 1, *A* and *B*, and Video 1). GFP-DGKβ was mainly localized on the plasma membrane before stimulation. Among type I DGK, only GFP-DGKβ accumulated without oscillation at the phagosomal cup, but not at the closed phagosome, during ingestion of BIgG. Accumulation of GFP-DGKβ briefly persisted at the plasma membrane where BIgG was ingested after closure of the phagosome (Fig. 1*C* and Video 2). More than 85% of the cells showed the accumulation of βI PKC-GFP, εPKC-GFP, and GFP-DGKβ (βI PKC-GFP < εPKC-GFP). Control beads (BBSA) were rarely phagocytosed by 6-3 cells (BBSA, 0.5 ± 0.1 per cell; BIgG, 8.4 ± 1.3 per cell), and did not cause any accumulation of above-mentioned molecules.

Different accumulation of βI and εPKC-GFP in FcγR-mediated phagocytosis

The time courses and patterns of the accumulation of βI PKC-GFP and εPKC-GFP were quite different. Localization times

were calculated and defined as T_1, time from the first concentration of PKC-GFP at the phagosomal cup until closure of the phagosome; T_2, time from closure of the phagosome until the signal returned to cytosolic levels; and T_t, $T_1 + T_2$. A repetitive accumulation of βI PKC-GFP was observed at the phagosomal cup and subsequently at the phagosome (19 of 22 cells; Fig. 1*A* and Video 1). The oscillatory accumulation of βI PKC-GFP occurred from 1 to 4 times (1, $n = 2$; 2, $n = 6$; 3, $n = 7$; and 4, $n = 4$) and was divided into two patterns; 1) accumulation only at the phagosomal cup, and 2) accumulation at both the cup and the phagosome. In accumulation pattern 2, T_1, T_2, and T_t were 24 ± 5, 21 ± 4, and 46 ± 7 s, respectively ($n = 10$). In contrast, εPKC-GFP accumulated at the phagosomal cup/phagosome without oscillation, and persisted longer (T_1, 26 ± 6 s; T_2, 93 ± 19 s; T_t, 119 ± 19 s; $n = 10$; Fig. 1*B*).

We used MARCKS-GFP as an indicator of the active PKC. MARCKS-GFP is constitutively present on the plasma membrane in an unphosphorylated form and is released from the membrane upon phosphorylation by PKC (19). In the present study, the loss of membrane-associated MARCKS-GFP was observed only at regions of the plasma membrane containing BIgG (Fig. 1*D*). Although not definitive, this evidence is consistent with the presence of active PKC in the forming phagosome. This conclusion is strengthened by the use of a mutant MARCKS-GFP that cannot be phosphorylated by PKC (19). This mutant MARCKS-GFP accumulated and was retained at the phagosomal cup and the forming phagosomal membrane during internalization of BIgG (Fig. 1*E*).

To validate that the GFP constructs mimic their endogenous counterparts, we measured the translocation of endogenous βI and εPKC during FcγR-mediated phagocytosis in 6-3 cells. βI and εPKC increased in the membrane fraction of nontransfected 6-3 cells in a time-dependent fashion (Fig. 2). Similar to the results with GFP conjugates, the increase in membrane-associated εPKC was sustained longer than that of βI PKC (Fig. 2).

Mechanism of oscillatory accumulation of βI PKC-GFP in FcγR-mediated phagocytosis

We have reported that εPKC, but not cPKC, enhances the rate of BIgG uptake, and that inhibition of εPKC causes ~50% inhibition of FcγR-mediated phagocytosis (3). Therefore, we focused on clarifying the accumulation/activation mechanism and the functional role of βI PKC in the present study. The accumulation of βI PKC-GFP was abolished by 2 μM U73122, an inhibitor of PLC (9), but not its inactive analog, U73343 (Fig. 3*A*). Pretreatment with R59949, an inhibitor of type I DGK, enhanced the accumulation of βI PKC-GFP, and induced the translocation of βI PKC-GFP to the plasma membrane (Fig. 3*B*). This result was confirmed by fractionation experiments. Treatment with R59949 increased the amount of membrane-associated βI PKC (Fig. 3, *C* and *D*).

To clarify the mechanism of βI PKC-GFP oscillations, $[Ca^{2+}]_i$ increase, and the production of DAG during phagocytosis were examined. One phagocytic event resulted in 1–4 $[Ca^{2+}]_i$ oscillations as determined by an increase in the 340:380 ratio of Fura 2 fluorescence (Fig. 4*A* and Video 3). Pretreatment with 2 μM U73122, but not U73343, significantly suppressed the amplitude of $[Ca^{2+}]_i$ increase (Fig. 4*B*). δPKC(C1)-GFP, a DAG indicator (9), transiently accumulated at the phagosomal cup/phagosome without oscillation (Fig. 4*C*). U73122 inhibited the accumulation of δPKC(C1)-GFP in dose-dependent manner (data not shown). Both Ca^{2+} and DAG are necessary for the full-activation of cPKC on the membrane (25). Taken together, these results are consistent with a model in which the oscillations of βI PKC-GFP during

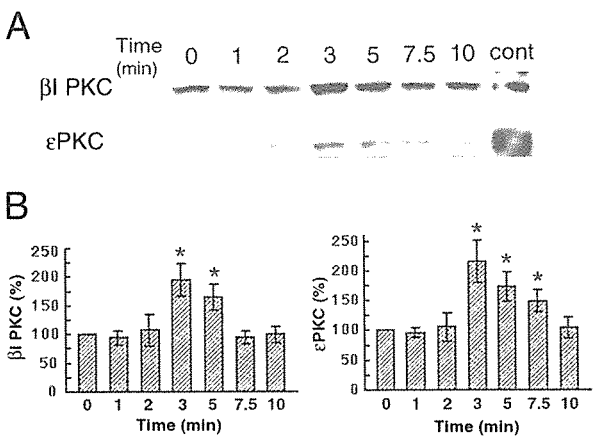

FIGURE 2. Translocation of endogenous βI and εPKC to the membrane fraction during synchronized phagocytosis of BIgG. *A*, βI PKC in the membrane fraction increases from 3 to 5 min. The increase of εPKC in the membrane fraction is sustained longer than that of βI PKC from 3 to 7.5 min. Representative of four experiments; cont, positive control from rat brain. *B*, Quantitation of membrane-associated βI PKC and εPKC during synchronized phagocytosis. Quantitative image analysis was performed using a NIH image. *, Significantly greater than 0 time point; $p < 0.05$.

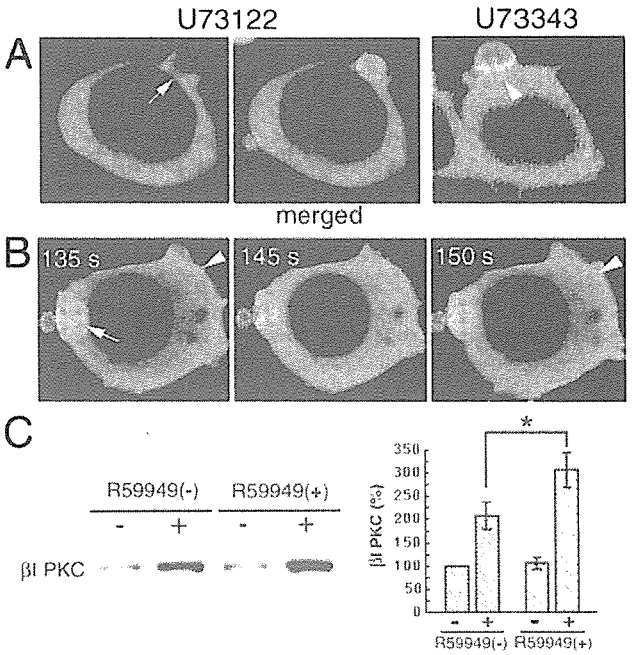

FIGURE 3. Mechanism of accumulation of βI PKC in FcγR-mediated phagocytosis. *A*, The accumulation of βI PKC-GFP is blocked by pretreatment with 2 μM U73122 for 15 min (arrow; $n = >9$). In contrast, βI PKC-GFP is recruited normally to the phagosomal cup in the presence of 2 μM U73343 for 15 min (arrowhead; $n = >9$). *B*, Pretreatment with 50 μM R59949 for 15 min enhances the accumulation of βI PKC-GFP (arrow; $n = >9$). It also induces the translocation of βI PKC-GFP to the plasma membrane (arrowheads). *C*, Translocation of endogenous βI PKC to the membrane fraction during synchronized phagocytosis of BIgG is enhanced by 10 μM R59949. With the DGK inhibitor (R59949(+)), the maximum increase of βI PKC in the membrane fraction (6 min) was greater than that without the inhibitor (R59949(−) 4 min). Representative of four experiments; −, without BIgG stimulation; +, with BIgG stimulation. *D*, Quantitation of maximum increase of membrane-associated βI PKC with or without R59949 during synchronized phagocytosis. Quantitative image analysis was performed using a NIH image. *, $p < 0.05$; −, without BIgG stimulation; +, with BIgG stimulation.

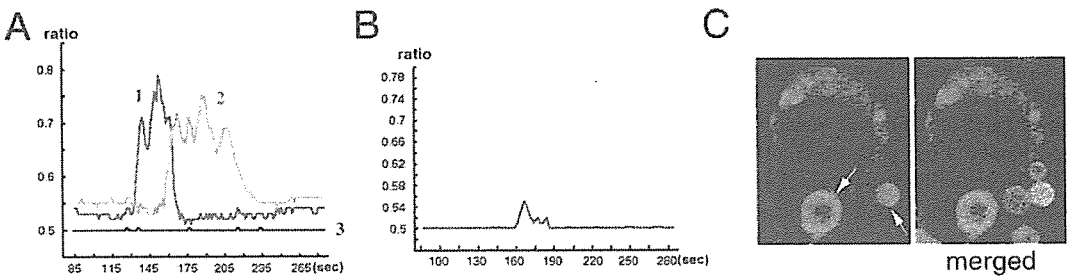

FIGURE 4. Mechanism of oscillatory accumulation of βI PKC in FcγR-mediated phagocytosis. *A*, Quantitation of $[Ca^{2+}]_i$ oscillations during phagocytosis (n = >20). The cells corresponding to each profile are identified in Video 3 (supporting information). Cell 1 (blue line) showing two $[Ca^{2+}]_i$ oscillations (duration, 39 s) and cell 2 (purple line) generating four oscillations (duration, 60 s) each ingested one BIgG (as determined by phase-contrast microscopy after the measurement). Cell 3 (black line) shows no $[Ca^{2+}]_i$ increase because there was no phagocytosis. *B*, Pretreatment with 2 μM U73122 for 15 min significantly suppresses the amplitude of $[Ca^{2+}]_i$ increase (n = >9). *C*, δPKC(C1)-GFP, a DAG indicator, accumulates at the phagosome (arrows; n = >20).

BIgG ingestion are due to parallel $[Ca^{2+}]_i$ oscillations in cooperation with localized DAG production at the phagosomal cup/phagosome.

O_2^- production during FcγR-mediated phagocytosis

We measured O_2^- production in 6-3 cells during FcγR-mediated phagocytosis using a superoxide dismutase-inhibitable luminal-based detection system (21).

O_2^- production was abolished by 100 nM Gö6976, a selective inhibitor of cPKC (1.64 ± 0.1% of uninhibited controls) or 2 μM U73122, a PLC inhibitor (0.1 ± 0.0%). In contrast, 10 μM R59949 increased O_2^- production 4.37-fold (Table I). O_2^- production was inhibited by Gö6976 (0–300 nM) and enhanced by R59949 (0–10 μM) in a dose-dependent manner (Fig. 5). As βI PKC is the only cPKC associated with phagosomes in 6-3 cells, and Gö6976 effectively blocks O_2^- production, this data supports a model in which βI PKC mediates O_2^- release. The fact that U73122 mimics the Gö6976 effect with respect to the inhibition of O_2^- release is consistent with the activation of βI PKC via PLC-derived DAG and IP_3-mediated rise in $[Ca^{2+}]_i$. However, Gö6976 did not affect the accumulation of βI PKC (Table I), providing evidence that βI PCK activity, rather than localization, is necessary for O_2^- production.

Oxidant-producing site during FcγR-mediated phagocytosis

PKC phosphorylates $p47^{phox}$, acting as the major activating kinase for the NADPH oxidase (11). We tested the hypothesis that accumulation of βI PKC corresponds with the temporal localization of $p47^{phox}$. In 6-3 cells expressing GFP-$p47^{phox}$ and $p67^{phox}$, GFP-$p47^{phox}$ accumulated at the phagosomal cup/phagosome without oscillation (T_1, 65 ± 7; n = 5; Fig. 6*A*), but not on nontarget-associated plasma membranes. GFP-$p47^{phox}$(R193W), which does not bind to $p22^{phox}$ nor produce O_2^- (20), did not accumulate at the phagosomal cup/phagosome (Fig. 6*B*). The accumulation of GFP-$p47^{phox}$ was not enhanced by pretreatment with R59949 (data not shown).

Because βI PKC-GFP and GFP-$p47^{phox}$ accumulated at the phagosomal cup/phagosome during phagocytosis of BIgG, we hypothesized that NADPH oxidase could be activated only at the site of PKC accumulation. We used electron microscopy to visualize the intracellular site of H_2O_2 production (dismutated from O_2^- generated by NADPH oxidase) in response to either BIgG or PMA. In 6-3 cells, the reaction product stimulated by BIgG was detected only at the phagosome (Fig. 7*A*), while that by PMA was at the intracellular granules (Fig. 7*B*). No reaction precipitate was found in cells incubated in the absence of $CeCl_3$, BIgG, or PMA (data not shown). These results show that oxidant production during FcγR-stimulated phagocytosis initiates at the phagosomal cup/phagosome, but not at the intracellular granules.

Discussion

This study and one recent report showed that NADPH oxidase functions in the microglia of the CNS (26). The present study is a first report of the visualizing the signal transduction pathway during FcγR-mediated respiratory burst at the cellular level in microglia. There are many reports that multiple PKC isoforms (α, β, δ, ε and ζPKC) involved in phagocytosis (22, 27). In 6-3 microglial cells, PKC isoforms α, βI, δ, ε, η, and ζPKC were expressed, and only βI and εPKC-GFP, but not α, δ, η, or ζPKC-GFP, accumulated at the phagosomal cup/phagosome, but not on the plasma membrane, during phagocytosis of BIgG. These findings are intriguing that receptor ligation not only controls which PKC isoform translocates but also the membranes to which they localize. There is a report that dominant negative αPKC impaired FcγR-mediated phagocytosis in RAW macrophages (28). However, we have reported that cPKC mediates the FcγR-stimulated respiratory burst, and that nPKC is necessary for phagocytosis in RAW cells (22). More recently, we have demonstrated that εPKC, but not cPKC, enhances the rate of BIgG uptake, and that inhibition of εPKC causes ~50% inhibition of FcγR-mediated phagocytosis (3). In microglia, no accumulation of αPKC-GFP was observed during BIgG ingestion, and a selective inhibitor of cPKC did not

Table I. *Effects of PKC, PLC, and DGK inhibitors on 6-3 cell function in FcγR-mediated phagocytosis*[a]

	Gö6976	U73122	U73343	R59949
O_2^- production	1.64 ± 0.1 %**	0.1 ± 0.0 %**	110.4 ± 2.2 %*	436.9 ± 16.1 %**
Phagocytosis	97.5 ± 9.0 %	65.9 ± 6.6 %**	98.0 ± 5.2 %	118.6 ± 9.3 %**
βI PKC accumulation	+	−	+	++

[a] Results are presented as a percentage of uninhibited controls (means ± SD %; $n \geq 4$). +, ++, and − means normal, enhanced, and abolished accumulation, respectively. Gö6976 was used at 500 nM (100 nM for measurement of O_2^-) for −15 min prior to the addition of stimulus. Pretreatment with 2 μM U73122 and U73343 was done for 15 min: R59949 was used at 10 μM for 15 min. O_2^- production was determined using a luminol-based detection system. See text for details. **, $p < 0.01$ and *, $p < 0.05$.

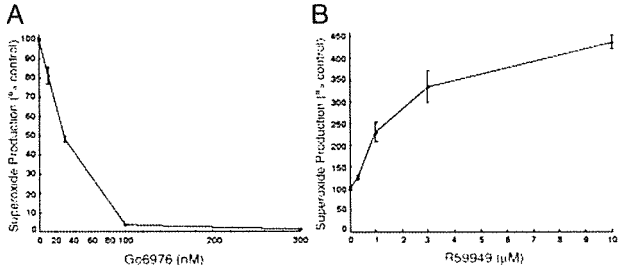

FIGURE 5. Dose-dependent inhibition of O_2^- production by Gö6976 (*A*) or enhancement by R59949 (*B*) in FcγR-mediated phagocytosis. Data are obtained from at least four independent experiments and expressed as means ± SD.

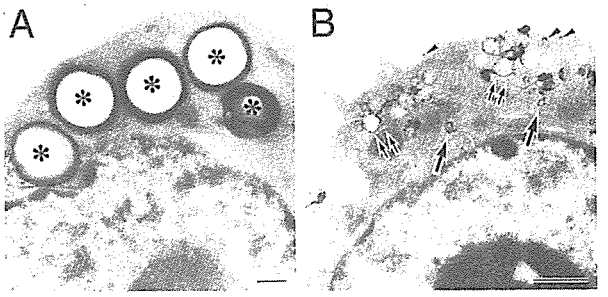

FIGURE 7. Representative electron micrographs of the oxidant production site in response to BIgG (latex; *A*; $n = 15$), and PMA (*B*; $n = 9$). The former reveals the reaction product only around BIgG in the phagosome (asterisks). The latter shows the reaction product at intracellular compartments consisting of vesicles (arrows), vacuoles (double arrows), and smaller vesicles (arrowheads) near the plasma membrane. Bars, 1 μm.

change the phagocytosis (Table I). Taken together, FcγR efficiently couples to βI PKC to facilitate O_2^- production in microglia. In addition, accumulation of εPKC had a good correlation with BIgG uptake in microglia as macrophages (our unpublished data). In the present study, we also showed the apparent differences of the accumulation patterns between βI PKC-GFP and εPKC-GFP. Two signals, one the locally produced DAG at the phagosomal cup/phagosome by PLCγ and the other the $[Ca^{2+}]_i$ oscillations by PLCγ, acting in concert are required for activation of βI PKC during FcγR-mediated phagocytosis. In an earlier study, stepwise phosphorylation of $p47^{phox}$ by PMA was indeed reported: although the final phosphorylation event of $p47^{phox}$ initiating O_2^- production occurs at membrane components, the first phosphorylation of $p47^{phox}$ promoting its translocation to membrane components primarily occurs in cytosol (29). We showed that accumulation of $p47^{phox}$ was not oscillatory, supporting a model that phosphorylated $p47^{phox}$ tightly associates with membrane (29). Recently, Dewitt et al. (30) reported that the first $[Ca^{2+}]_i$ increase is not sufficient for O_2^- production. The possibility exists that the oscillatory signal by βI PKC between the phagosomal cup/phagosome and cytosol are used for both initialization of membrane translocation of $p47^{phox}$ in cytosol and tight association of $p47^{phox}$ to membrane and full activation of the NADPH oxidase at membrane. However, the physiological contributions of the oscillatory accumulation of βI PKC is presently unclear.

In vitro, $p47^{phox}$ is phosphorylated on 8–10 serine residues within its C-terminal region by different types of protein kinases; one or more PKC family members are indicated to play a major role (31). Phosphopeptide mapping of $p47^{phox}$ showed that α, β, and δPKC phosphorylated all major peptides, although δPKC was less active toward some peptides; phosphorylation by ζPKC was only a few peptides (11). Using neutrophils from βPKC null mice, Dekker et al. (5) reported that the lack of βPKC decreased the amount of O_2^- production by 50% stimulated by BIgG and PMA, and they also demonstrated a significant inhibition of O_2^- production stimulated by PMA and IgG-opsonized bacteria in human neutrophils treated with a βPKC-specific inhibitor (5). It was also reported that a similar degree of inhibition of O_2^- production by PMA, immune complex, and fMLP in human HL60 cells using an antisense method *(32)*. In contrast, αPKC, but not βPKC, is involved in O_2^- production by BIgG (22) and by opsonized zymosan (33), in monocytes. Although apparently disparate, these results suggest that βPKC contributes to the respiratory burst in neutrophils while αPKC performs this function in monocytes. The present study is consistent with microglia using a neutrophil-like pathway for PKC regulation of O_2^- production. Furthermore, recent reports show that βPKC and δPKC bind to $p47^{phox}$ in intact neutrophils stimulated by PMA with different time courses (34), and ζPKC participates in the fMLP-induced, but not PMA-induced, respiratory burst (35). It was also reported that ζPKC accumulated on the phagosome during ingestion of *Helicobacter pylori*, but not IgG-opsonized *H. pylori* (36), in monocytes. Thus, it is likely that different receptors are coupled to the specialized signaling networks and use different PKC isoforms. Taken together,

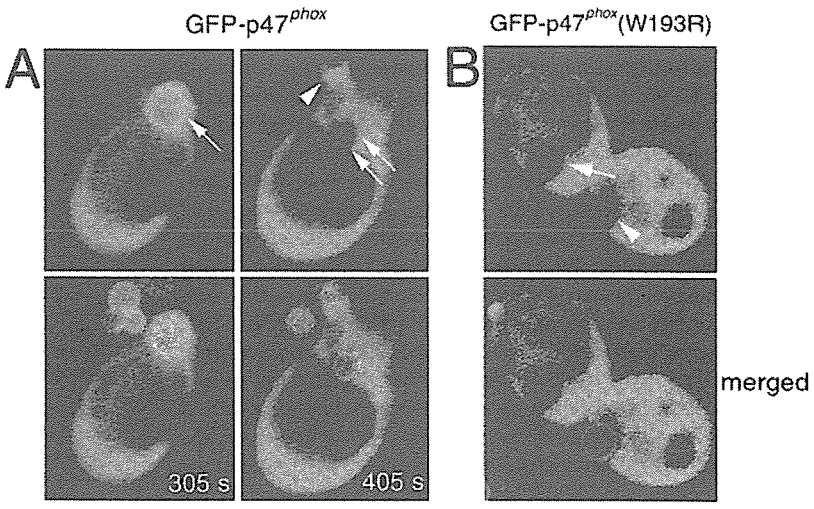

FIGURE 6. Accumulation of $p47^{phox}$ during FcγR-mediated phagocytosis. *A*, At 305 s, GFP-$p47^{phox}$ accumulation is apparent at the phagosome (arrow). By 405 s, the accumulation has disappeared (double arrows); weak accumulation of GFP-$p47^{phox}$ at a forming phagosomal cup is indicated by the arrowhead. Translocation of GFP-$p47^{phox}$ to the plasma membrane is not observed ($n = >12$). *B*, GFP-$p47^{phox}$(R193W) does not accumulate at any time point (arrow, phagosome; arrowhead, phagosomal cup; $n = >12$).

use of PKC isoform likely is determined by both the cell type and the stimulus.

O_2^- can be produced either extracellularly or within the phagosome during phagocytosis. Extracellular O_2^- is thought to originate from either the phagosomal cup or the plasma membrane. In the present study, during the ingestion of BIgG, βI PKC-GFP and GFP-$p47^{phox}$ translocated to the phagosomal cup/phagosome, but not to the plasma membrane. These results indicate that the extracellular O_2^- primarily originates from the phagosomal cup. DAG is one of the key lipid mediators in O_2^- production (37, 38). Inhibition of DGK with R59949 significantly enhanced O_2^- production and induced the translocation of βI PKC-GFP to the plasma membrane in addition to the enhanced accumulation at the phagosomal cup/phagosome. However, the accumulation of GFP-$p47^{phox}$ was not enhanced by pretreatment with R59949, this result suggests that DAG may not be primarily associated with the translocation of $p47^{phox}$ and enhanced O_2^- production may be primarily from the enhanced accumulation of βI PKC at the phagosomal cup/phagosome. Furthermore, DGKβ accumulated on the forming phagosome, but not at the closed phagosome, while βI PKC and $p47^{phox}$ accumulated both at the phagosomal cup and phagosome. Thus, DGKβ which is localized on the plasma membrane in resting states, accumulates on the forming phagosome, and briefly stays at the phagocytosis-involved plasma membrane after closure of the phagosome, likely plays an important role in control of excessive secretion of O_2^- to the extracellular milieu through regulation of βI PKC activation during phagocytosis rather than termination of O_2^- production. This is consistent with a report that termination of O_2^- production correlated with dissociation of $p47^{phox}$/$p67^{phox}$ complex from the phagosome (39). Because βI PKC accumulated at the phagosomal cup from initiation of phagocytosis and inhibition of βI PKC showed a profound decrease of O_2^- production, βI PKC most likely plays a key role for initiation of respiratory burst, at least. Other pathways, such as PI3K pathway, likely contribute to the later stage of O_2^- production (40). In agreement with this idea, GFP-tagged PX domain of $p40^{phox}$, a phosphatidylinositol 3-phosphate indicator, accumulated at the phagosome only after closure of the phagosome (our unpublished data).

It has been reported that cytochrome b_{558} is primarily localized on intracellular granules (~80%) in neutrophils (41). Recently, it was reported that O_2^- production stimulated by PMA initially takes place at intracellular granules, followed by fusion of these granules with the plasma membrane, resulting in the delivery of O_2^- into the extracellular milieu (13, 14). However, because βI PKC-GFP and GFP-$p47^{phox}$ accumulated at the phagosomal cup/phagosome in this study, we hypothesized that NADPH oxidase could be activated primarily at the phagosomal cup/phagosome during FcγR-mediated phagocytosis in microglia. Our present results using electron microscopy supported that oxidant production during FcγR-stimulated phagocytosis initiates at the phagosomal cup/phagosome where DAG is locally formed during BIgG ingestion, but not at the intracellular granules. In contrast, consistent with previous reports, PMA caused the oxidant production at the intracellular granules. We propose that O_2^- production during FcγR-stimulated phagocytosis begins at the phagosomal cup/phagosome through phosphorylation of $p47^{phox}$ by cPKC. Although microglia use βPKC as neutrophils do, and macrophages use αPKC, the basis of this model may be adapted to all phagocytes in FcγR-stimulated phagocytosis. In support of our results, it was reported that, based on stoichiometry, O_2^- is formed at the phagosomal cup/phagosome during phagocytosis of opsonized zymosan in neutrophils (42). When phagocytosis is blocked by cytochalasin B, O_2^- is formed at the phagosomal cup (cell-zymosan interface) only and secreted into the extracellular milieu (S. Kanegasaki, Tokyo University, unpublished observation). Microglia had only about one-tenth capacity for O_2^- production compared with neutrophils. Further elucidation, especially about the assembly of NADPH oxidase complex during FcγR-stimulated phagocytosis at the cellular level, is required.

Acknowledgments

We thank Dr. Kaoru Goto (Yamagata University School of Medicine, Yamagata, Japan) for providing the cDNA for rat DGKβ.

References

1. Greenberg, S., and S. Grinstein. 2002. Phagocytosis and innate immunity. *Curr. Opin. Immunol. 14:136.*
2. Bard, F., C. Cannon, R. Barbour, R. L. Burke, D. Games, H. Grajeda, T. Guido, K. Hu, J. Huang, K. Johnson-Wood, et al. 2000. Peripherally administered antibodies against amyloid β-peptide enter the central nervous system and reduce pathology in a mouse model of Alzheimer disease. *Nat. Med. 6:916.*
3. Larsen, E. C., T. Ueyama, P. M. Brannock, Y. Shirai, S. Saito, C. Larsson, D. J. Loegering, P. B. Weber, and M. R. Lennartz. 2002. A role for PKC-ε in FcγR-mediated phagocytosis by RAW 264.7 cells. *J. Cell Biol. 159:939.*
4. Leitges, M., C. Schmedt, R. Guinamard, J. Davoust, S. Schaal, S. Stabel, and A. Tarakhovsky. 1996. Immunodeficiency in protein kinase Cβ-deficient mice. *Science 273:788.*
5. Dekker, L. V., M. Leitges, G. Altschuler, N. Mistry, A. McDermott, J. Roes, and A. W. Segal. 2000. PKC-β contributes to NADPH oxidase activation in neutrophils. *Biochem. J. 347(Pt. 1):285.*
6. Castrillo, A., D. J. Pennington, F. Otto, P. J. Parker, M. J. Owen, and L. Bosca. 2001. PKCε is required for macrophage activation and defense against bacterial infection. *J. Exp. Med. 194:1231.*
7. Kanoh, H., K. Yamada, and F. Sakane. 2002. Diacylglycerol kinases. *J. Biochem. 131:629.*
8. Bokoch, G. M., and U. G. Knaus. 2003. NADPH oxidases: not just for leukocytes anymore! *Trends Biochem. Sci. 28:502.*
9. Botelho, R. J., M. Teruel, R. Dierckman, R. Anderson, A. Wells, J. D. York, T. Meyer, and S. Grinstein. 2000. Localized biphasic changes in phosphatidylinositol-4,5-bisphosphate at sites of phagocytosis. *J. Cell Biol. 151:1353.*
10. Babior, B. M. 1999. NADPH oxidase: an update. *Blood 93:1464.*
11. Fontayne, A., P. M. Dang, M. A. Gougerot-Pocidalo, and J. El-Benna. 2002. Phosphorylation of $p47^{phox}$ sites by PKC α, βII, δ, and ζ. *Biochemistry 41:7743.*
12. Hoyal, C. R., A. Gutierrez, B. M. Young, S. D. Catz, J. H. Lin, P. N. Tsichlis, and B. M. Babior. 2003. Modulation of $p47^{phox}$ activity by site-specific phosphorylation: Akt-dependent activation of the NADPH oxidase. *Proc. Natl. Acad. Sci. USA 100:5130.*
13. Kobayashi, T., J. M. Robinson, and H. Seguchi. 1998. Identification of intracellular sites of superoxide production in stimulated neutrophils. *J. Cell Sci. 111:81.*
14. Brown, G. E., M. Q. Stewart, H. Liu, V. L. Ha, and M. B. Yaffe. 2003. A novel assay system implicates PtdIns(3,4)P(2), PtdIns(3)P, and PKCδ in intracellular production of reactive oxygen species by the NADPH oxidase. *Mol. Cell. 11:35.*
15. Sawada, M., F. Imai, H. Suzuki, M. Hayakawa, T. Kanno, and T. Nagatsu. 1998. Brain-specific gene expression by immortalized microglial cell-mediated gene transfer in the mammalian brain. *FEBS Lett. 433:37.*
16. Kanzawa, T., M. Sawada, K. Kato, K. Yamamoto, H. Mori, and R. Tanaka. 2000. Differentiated regulation of allo-antigen presentation by different types of murine microglial cell lines. *J. Neurosci. Res. 62:383.*
17. Inoue, H., M. Sawada, A. Ryo, H. Tanahashi, T. Wakatsuki, A. Hada, N. Kondoh, K. Nakagaki, K. Takahashi, A. Suzumura, et al. 1999. Serial analysis of gene expression in a microglial cell line. *Glia 28:265.*
18. Shirai, Y., S. Segawa, M. Kuriyama, K. Goto, N. Sakai, and N. Saito. 2000. Subtype-specific translocation of diacylglycerol kinase α and γ and its correlation with PKC. *J. Biol. Chem. 275:24760.*
19. Ohmori, S., N. Sakai, Y. Shirai, H. Yamamoto, E. Miyamoto, N. Shimizu, and N. Saito. 2000. Importance of PKC targeting for the phosphorylation of its substrate, MARCKS. *J. Biol. Chem. 275:26449.*
20. Sumimoto, H., K. Hata, K. Mizuki, T. Ito, Y. Kage, Y. Sakaki, Y. Fukumaki, M. Nakamura, and K. Takeshige. 1996. Assembly and activation of the phagocyte NADPH oxidase. *J. Biol. Chem. 271:22152.*
21. Kuribayashi, F., H. Nunoi, K. Wakamatsu, S. Tsunawaki, K. Sato, T. Ito, and H. Sumimoto. 2002. The adaptor protein $p40^{phox}$ as a positive regulator of the superoxide-producing phagocyte oxidase. *EMBO J. 21:6312.*
22. Larsen, E. C., J. A. DiGennaro, N. Saito, S. Mehta, D. J. Loegering, J. E. Mazurkiewicz, and M. R. Lennartz. 2000. Differential requirement for classic and novel PKC isoforms in respiratory burst and phagocytosis in RAW 264.7 cells. *J. Immunol. 165:2809.*
23. Briggs, R. T., D. B. Drath, M. L. Karnovsky, and M. J. Karnovsky. 1975. Localization of NADH oxidase on the surface of human polymorphonuclear leukocytes by a new cytochemical method. *J. Cell Biol. 67:566.*
24. Kobayashi, T., E. Garcia del Saz, J. Hendry, and H. Seguchi. 1999. Detection of oxidant producing-sites in glutaraldehyde-fixed human neutrophils and eosinophils stimulated with PMA. *Histochem. J. 31:181.*
25. Oancea, E., and T. Meyer. 1998. PKC as a molecular machine for decoding calcium and diacylglycerol signals. *Cell 95:307.*

26. Lavigne, M. C., H. L. Malech, S. M. Holland, and T. L. Leto. 2001. Genetic requirement of $p47^{phox}$ for superoxide production by murine microglia. *FASEB J. 15:285.*
27. Sergeant, S., and L. C. McPhail. 1997. Opsonized zymosan stimulates the redistribution of protein kinase C isoforms in human neutrophils. *J. Immunol. 159:2877.*
28. Breton, A., and A. Descoteaux. 2000. Protein kinase C-α participates in FcγR-mediated phagocytosis in macrophages. *Biochem. Biophys. Res. Commun. 276:472.*
29. Rotrosen, D., and T. L. Leto. 1990. Phosphorylation of neutrophil 47-kDa cytosolic oxidase factor: translocation to membrane is associated with distinct phosphorylation events. *J. Biol. Chem. 265:19910.*
30. Dewitt, S., I. Laffafian, and M. B. Hallett. 2003. Phagosomal oxidative activity during β_2 integrin (CR3)-mediated phagocytosis by neutrophils is triggered by a non-restricted Ca^{2+} signal: Ca^{2+} controls time not space. *J. Cell Sci. 116:2857.*
31. El Benna, J., R. P. Faust, J. L. Johnson, and B. M. Babior. 1996. Phosphorylation of the respiratory burst oxidase subunit $p47^{phox}$ as determined by two-dimensional phosphopeptide mapping: phosphorylation by protein kinase C, protein kinase A, and a mitogen-activated protein kinase. *J. Biol. Chem. 271:6374.*
32. Korchak, H. M., M. W. Rossi, and L. E. Kilpatrick. 1998. Selective role for β-protein kinase C in signaling for O_2^- generation but not degranulation or adherence in differentiated HL60 cells. *J. Biol. Chem. 273:27292.*
33. Li, Q., V. Subbulakshmi, A. P. Fields, N. R. Murray, and M. K. Cathcart. 1999. PKC α regulates human monocyte O_2^- production and low density lipoprotein lipid oxidation. *J. Biol. Chem. 274:3764.*
34. Reeves, E. P., L. V. Dekker, L. V. Forbes, F. B. Wientjes, A. Grogan, D. J. Pappin, and A. W. Segal. 1999. Direct interaction between $p47^{phox}$ and PKC. *Biochem. J. 344(Pt. 3):859.*
35. Dang, P. M., A. Fontayne, J. Hakim, J. El Benna, and A. Perianin. 2001. Protein kinase C ζ phosphorylates a subset of selective sites of the NADPH oxidase component $p47^{phox}$ and participates in formyl peptide-mediated neutrophil respiratory burst. *J. Immunol. 166:1206.*
36. Allen, L. A., and J. A. Allgood. 2002. Atypical PKC-ζ is essential for delayed phagocytosis of *Helicobacter pylori*. *Curr. Biol. 12:1762.*
37. Arnhold, J., S. Benard, U. Kilian, S. Reichl, J. Schiller, and K. Arnold. 1999. Modulation of luminol chemiluminescence of fMLP-stimulated neutrophils by affecting dephosphorylation and the metabolism of phosphatidic acid. *Luminescence 14:129.*
38. Erickson, R. W., P. Langel-Peveri, A. E. Traynor-Kaplan, P. G. Heyworth, and J. T. Curnutte. 1999. Activation of human neutrophil NADPH oxidase by phosphatidic acid or diacylglycerol in a cell-free system. *J. Biol. Chem. 274:22243.*
39. DeLeo, F. R., L. A. Allen, M. Apicella, and W. M. Nauseef. 1999. NADPH oxidase activation and assembly during phagocytosis. *J. Immunol. 163:6732.*
40. Karlsson, A., J. B. Nixon, and L. C. McPhail. 2000. PMA induces neutrophil NADPH-oxidase activity by two separate signal transduction pathways. *J. Leukocyte Biol. 67:396.*
41. Jesaitis, A. J., E. S. Buescher, D. Harrison, M. T. Quinn, C. A. Parkos, S. Livesey, and J. Linner. 1990. Ultrastructural localization of cytochrome *b* in the membranes of resting and phagocytosing human granulocytes. *J. Clin. Invest. 85:821.*
42. Makino, R., T. Tanaka, T. Iizuka, Y. Ishimura, and S. Kanegasaki. 1986. Stoichiometric conversion of oxygen to superoxide anion during the respiratory burst in neutrophils. *J. Biol. Chem. 261:11444.*

Available online at www.sciencedirect.com
SCIENCE DIRECT
Neuroscience Research 51 (2005) 73–80
Neuroscience Research
www.elsevier.com/locate/neures

Localization of cyclooxygenase-2 induced following traumatic spinal cord injury

Kayo Adachi[a], Yu Yimin[b], Kotaro Satake[b], Yukihiro Matsuyama[b], Naoki Ishiguro[b], Makoto Sawada[a], Yoko Hirata[c], Kazutoshi Kiuchi[c,*]

[a]*Joint Research Division for Therapies against Intractable Diseases, Institute for Comprehensive Medical Science, Fujita Health University, Toyoake, Aichi 470-1192, Japan*
[b]*Department of Orthopaedic Surgery, Nagoya University School of Medicine, Nagoya 466-8550, Japan*
[c]*Department of Biomolecular Science, Faculty of Engineering, Gifu University, 1-1 Yanagido, Gifu 501-1193, Japan*

Received 10 September 2003; accepted 4 October 2004

Abstract

Objective: Up-regulation of cyclooxygenase-2 (COX-2), a key enzyme in the synthesis of prostaglandins (PGs), is postulated to be involved in pathological processes of acute spinal cord injury (SCI). In the present study, we sought to clarify temporal and spatial expression patterns of the *COX-2* gene induced in the spinal cord after traumatic insults using a weight-drop technique.
Results: Reverse transcriptase-polymerase chain reaction (RT-PCR) revealed that COX-2 transcription in the spinal cord began to increase within 30 min, peaked at 3 h after injury. Western blotting analysis indicated that the deglycosylated COX-2 protein significantly increased 6 h after injury. Double-immunofluorescent staining analysis showed that COX-2 immunoreactivity was present only in endothelial cells of blood vessels, but not in neurons, astrocytes, monocytes, macrophages, or microglia 6 h after injury.
Conclusions: The results suggested that *COX-2* gene induction seems not to require any new protein synthesis and that its expression in endothelial cells may be a component of an inflammatory process after traumatic SCI.

Keywords: Cyclooxygenase-2; Endothelial cells; Pia matters; Blood vessels; Rat; Spinal cord injury; Weight-drop technique

1. Introduction

Cyclooxygenase (COX) is a rate-limiting enzyme that catalyzes steps in the prostaglandin biosynthesis of arachidonic acid to PGG_2 and then to PGH_2, which is an unstable and common precursor for all prostanoids; two distinct isoforms of COX have been cloned (Kujubu et al., 1991; DeWitt and Smith, 1998). COX-1 is constitutively expressed in most tissues (DeWitt, 1991), whereas COX-2 is undetectable in most mammalian tissues (Smith et al., 1996) but is induced in response to various cytokines (Kujubu and Herschman, 1992; O'Banion et al., 1992), growth factors (Sirois et al., 1993), and endotoxins (Feng et al., 1993). Recently, COX-2 induction in the central nervous system (CNS) by some stimuli, such as bacterial lipopolysaccharide (LPS) (Breder and Saper, 1996) and interleukin-1β (IL-1β) (Inoue et al., 1999; Serou et al., 1999) has been demonstrated, and it has been observed in various pathologic conditions, such as seizures (Yamagata et al., 1993), global ischemia-reperfusion (Nakayama et al., 1998), peripheral inflammation (Ichitani et al., 1997), and traumatic spinal cord injury (SCI)(Resnick et al., 1998; Tonai et al., 1999).

The pathological process in SCI is considered to consist of two steps: the primary mechanical injury and secondary damage induced by various biochemical reactions (Faden, 1993; Tator, 1995). In the secondary damage, numerous factors are thought to contribute at a molecular level to spinal cord impairment, and are derived from a reduction of microcirculation in tissue (Tator and Fehlings, 1991). We have previously reported the up-regulation of two genes; *iNOS* and *GDNF*, in the immediate early stage after SCI. NO

* Corresponding author. Tel.: +81 582932651; fax: +81 582301893.
E-mail address: kiuchi@biomol.gifu-u.ac.jp (K. Kiuchi).

0168-0102/$ – see front matter
doi:10.1016/j.neures.2004.10.007

produced by iNOS-positive macrophages seems to trigger apoptosis of any adjacent damaged cells during the early stage of traumatic SCI (Satake et al., 2000a), while GDNF induced in microglia and macrophage is considered to exert a protective effect on neurons following SCI (Satake et al., 2000b). Nuclear factor-κB (NF-κB) responsive elements are known to exist in the promoter region of the *COX-2* gene (Yamamoto et al., 1995; Jobin et al., 1998) as well as in *iNOS* (Chao et al., 1997; Nishiya et al., 2000; Madrigal et al., 2001) and *GDNF* genes (Tanaka et al., 2000). Recently it has been reported that COX-2 expression causes both pro- and anti-inflammatory process including the NF-κB-dependent transcription in epithelial cells (Poligone and Baldwin, 2001). Therefore, these three genes are considered to influence one another and the balance of their activities seems to determine neuronal survival or degeneration. However, the precise starting point of induction of the *COX-2* gene and the localization of COX-2 protein in the spinal cord following traumatic SCI still remain unclear. In the present study, using reverse transcriptase-polymerase chain reaction (RT-PCR), we determined the time course of *COX-2* gene induction and using double-immunofluorescent staining, we investigated whether COX-2 protein expression is up-regulated in neurons, astrocytes, macrophages, microglia or endothelial cells in rat spinal cord after traumatic SCI by a weight-drop technique.

2. Material and methods

2.1. Surgical procedure for traumatic SCI

Sprague–Dawley rats (8 weeks, male) were anesthetized with pentobarbital and laminectomies were performed at the T8–T10 level. Spinal cords were injured using the weight-drop technique according to Allen's method (Allen, 1914) with a slight modification. A plastic impounder (2-mm diameter) was placed gently on the exposed dura and a 10-g iron weight was dropped from a height of a 10 cm onto the impounder. The weight and impounder were immediately removed after impact and paravertebral muscle and skin were closed. Sham controls underwent the same operations but without spinal cord insult. Rats used in this study were treated strictly according to the NIH Guide for Care and Use of Laboratory Animals, and our protocol was approved by RIKEN.

2.2. RNA extraction and RT-PCR

Rats were again anesthetized with pentobarbital and their spinal cords from the top and bottom 1.5 cm of the lesion were removed at 30 min, 3 h, 6 h, 12 h, 1 day, 2 days, 3 days, and 1 weeks; similarly those of the sham controls (0 min and 3 h). They were immediately frozen with dry ice and stored at −80 °C until use. Total mRNA was prepared from cord segments using RNeasy Midi (Qiagen) and the resultant mRNA was reverse transcribed with oligo d(T) 12–18 using Superscript II (Invitrogen). This RT mixture was used as a template for PCR. PCRs were carried out in a GeneAmp PCR System 2400 (Applied Biosystems) using a protocol consisting of denaturation at 95 °C for 60 s, annealing at 60 °C for 60 s, and extension at 72 °C for 60 s in each of 35 cycles for COX-2 and 25 cycles for β-actin, respectively. The primer sets were COX-2; 5′-GAA CAA CAT TCC CTT CCT TCG-3′ and 5′-GAA GTT CCT TAT TTC CTT TCA CAC C-3′, and β-actin; 5′-TGT ATG CCT CTG GTC GTA CC-3′ and 5′-CAA CGT CAG ACT TCA TGA TGG-3′. The PCR products were electrophoresed through a 1.5% agarose gel containing ethidium bromide. Images were captured using a Gel Print 2000i/VGA (Bio Image), and the intensity ratio between the COX-2 and β-actin bands was determined using the computer software, Intelligent Quantifier (Bio Image).

2.3. Tissue preparation

Six hours after injury, rats were anesthetized with sodium pentobarbital (50 mg/kg) perfused through the ascending aorta with 4 ml of heparin (1000 U/ml in 0.9% NaCl) and with 20 ml of 4% (w/v) paraformaldehyde (PFA) in 0.1 M sodium phosphate buffer (PB), pH 7.4. Their spinal cords were removed and post-fixed for 4 h in 4% PFA at 4 °C. After cryoprotection in 30% sucrose for 3 days, they were embedded in OCT compound (Tissue TEK II, Miles), rapidly frozen in dry ice–acetone, and stored at −80 °C until

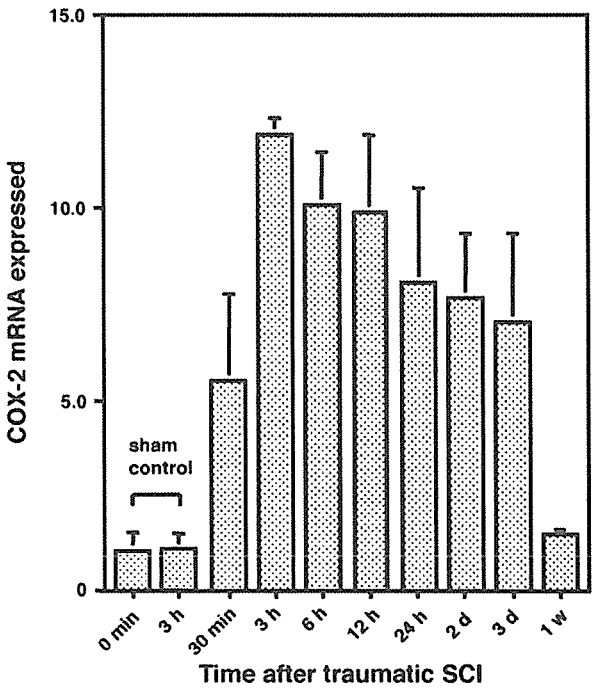

Fig. 1. COX-2 mRNA expression in sham controls and at various times after traumatic spinal cord injury. Data are expressed as the means ± S.E.M. ($n = 3$) of COX-2/β-actin mRNA ratios quantified using Intelligent Quantifier.

use. Seven micrometers of coronal frozen sections were cut on a cryostat JUNG CM 3000 (Lica), mounted onto silanized slides (DAKO), air-dried, and stored at −80 °C until were used for immunohistochemistry.

2.4. Western blotting

Rats were anesthetized with diethylether 6 h after spinal cord impaction and their spinal cord from the top and bottom 1.5 cm (100 mg) of the lesion were dissected, homogenized in 10 times of the sample buffer (62.5 mM Tris, pH 6.8, 2% SDS, 10% glycerol, 5% 2-mercaptethanol, and 0.01% bromophenol blue), lysed, and denatured. Five mircoliters of each sample was loaded on to an 8% SDS–polyacrylamide gel. Proteins were transferred to a nitrocellulose membrane. The membrane was probed with mouse monoclonal antibody to COX-2 (dilution: 1:100; Transduction) and proteins were detected using a chemiluminescent detection system (Amersham Bioscience).

2.5. Immunohistochemistry

Spinal cord sections were incubated in blocking solution (10% normal donkey serum with 0.4% Triton X-100 in PBS) for 30 min, COX-2 antibody for 48 h at 4 °C, and Cy3-conjugated donkey anti-rabbit IgG for 1 h. For double staining, the sections were incubated with the appropriate combination antibodies against COX-2, iNOS, or cell-specific monoclonal antibodies. After washing with PBS, they were stained with a combination of FITC-labeled anti-rabbit IgG or Cy3-labeled anti-mouse IgG for 1 h. They were rinsed in PBS, mounted with Fluoroguard (Bio Rad),

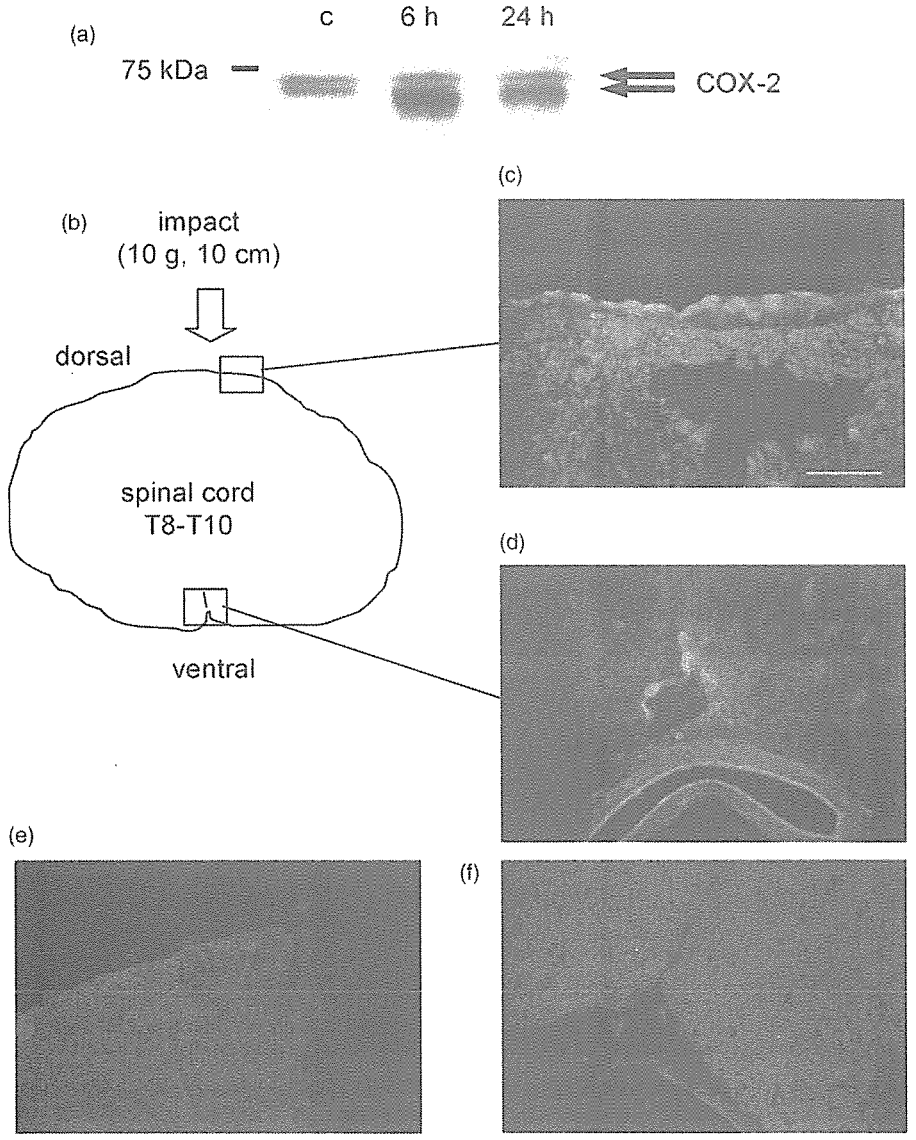

Fig. 2. (a) Western blot analysis of protein extracts obtained from spinal cord of rat 6 h and 24 h after traumatic spinal cord injury (SCI) and control rat. (b) A sketch of rat spinal cord (T8–T10) where each photograph of immunofluorescent staining specimen was obtained. Immunofluorescent staining for COX-2 in rat spinal cord around the perivascular zone (c and e) and pia matter (d and f); 6 h after traumatic SCI (c and d) or normal control (e and f). COX-2 positive cells were visualized with FITC-conjugated donkey antibody against rabbit IgG as a secondary antibody. Scale bar = 50 μm.

and examined under a fluorescent microscope with a camera attachment (Olympus).

2.6. Antibodies for immunohistochemistry

Rabbit anti-COX-2 polyclonal antibody was purchased from Cayman and used at 1:200 dilution. Mouse anti-COX-2 monoclonal antibody was purchased from Transduction and used at 1:100 dilution. Rabbit anti-iNOS polyclonal antibody was prepared using GST–iNOS (N-terminal) fusion protein as reported previously (Fan et al., 1995) and used at 1:250 dilution. Cell-specific monoclonal antibodies were purchased and used as described below: ED1, specific for monocyte, macrophage, and dendritic cells (BMA Biomedical) at 1:500; ED2, specific for macrophage (BMA Biomedical) at 1:500; OX42, specific for macrophage and microglia (BMA Biomedical) at 1:100; Cy3-conjugated glial fibrillary acidic protein (GFAP) for astrocyte (Sigma) at 1:400; MAP2, specific for neuron (Chemicon) at 1:200; and RECA-1, specific for endothelial cells (Monosan) at 1:200 Fluorescent secondary anti-mouse and rabbit antibodies (Chemicon) at 1:100 were also used.

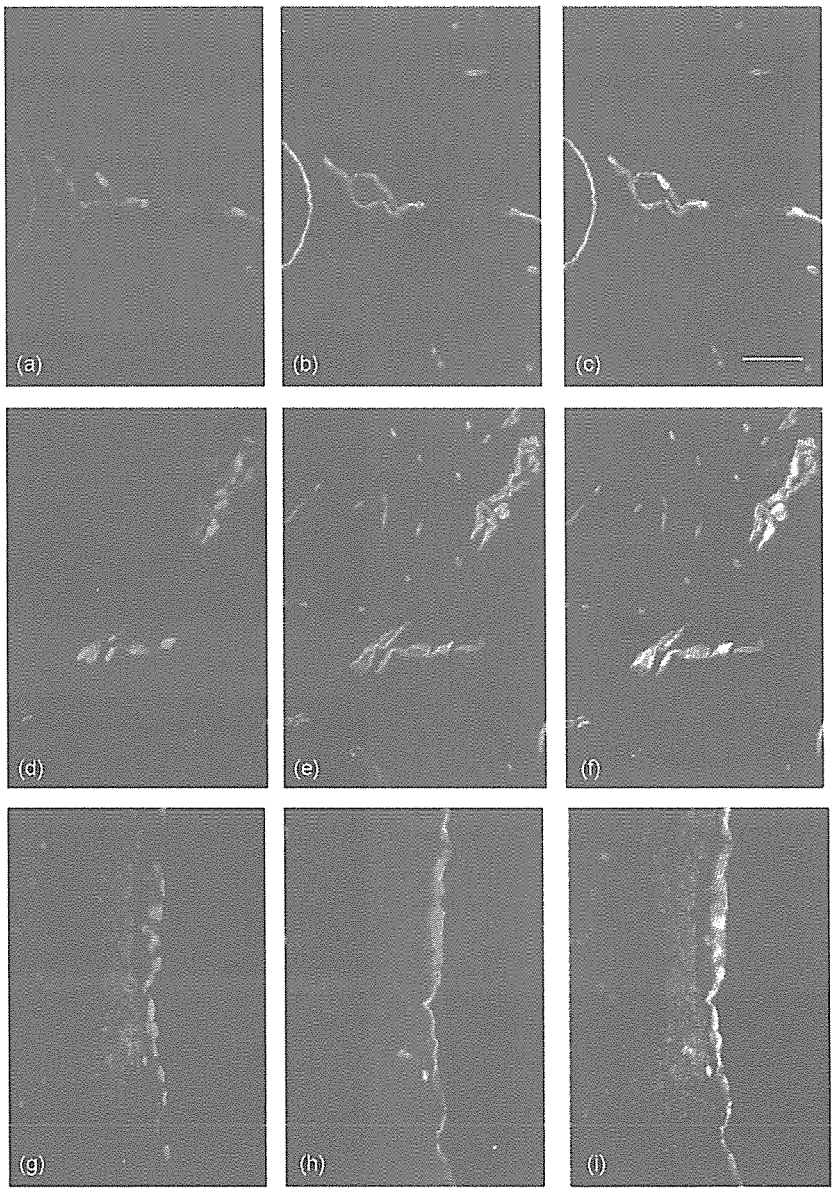

Fig. 3. Double-immunofluorescent staining of rat spinal cord, 6 h after traumatic SCI for COX-2 (green) and cell-specific markers (red). COX-2 positive cells were visualized with FITC-conjugated donkey antibody against rabbit IgG as a secondary antibody (a, d, g, j, m, p, s, and v). GFAP (n) was visualized using Cy3-conjugated mouse monoclonal antibody, and RECA-1 (b, e, and h), MAP2 (k), ED1 (q), ED2 (t), and OX-42 (w) immunoreactivities were visualized with Cy3-conjugated donkey antibody against mouse IgG as a secondary antibody. COX-2 positive cells were observed around the perivascular zone (b), the blood vessel (e), and pia matter (h), but did not coincide with MAP2 (k), GFAP (n), ED1 (q), ED2 (t), and OX42 (w) positive cells. COX-2 positive cells were shown in yellow by superimposing the two color images (c, f, and i). Scale bar = 50 μm. (For interpretation of the references to colour in this figure legend, the reader is referred to the web version of the article).

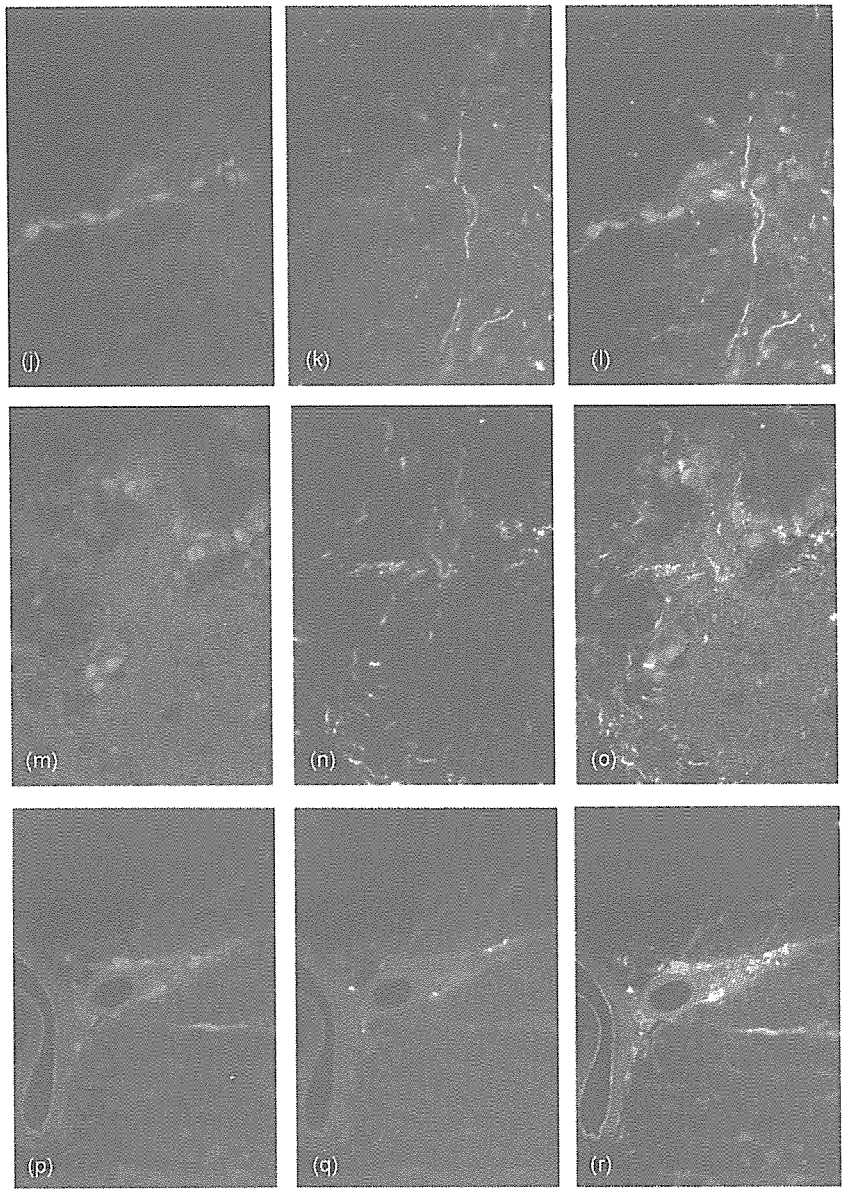

Fig. 3. (*Continued*).

3. Results

Hematoxylin–Eosin staining was performed to observe the spread of damage following weight drop impact on the rat spinal cord. Damage caused by traumatic SCI spread from the dorsal white matter to central gray matter 6 h after the injury and even the ventral gray matter began to become cavernous 3 days after the injury (data not shown, Satake et al., 2000a). First, we confirmed the time-course of COX-2 induction in the spinal cord after the injury using semi-quantitative RT-PCR. COX-2 mRNA began to increase within 30 min, peaked at 3 h, gradually began to decline at 6 h, and returned to basal levels about 1 week after the injury (Fig. 1). Sequence analysis confirmed that the 209-bp band corresponded to the rat COX-2 cDNA fragment. Next, COX-2 protein level and localization were examined in the spinal cord after traumatic SCI. Western blotting analysis showed that COX-2 protein significantly increased 6 h and remained at a high level until 24 h after the injury compared with those in control animals (Fig. 2a). Although COX-2 protein has been previously reported to compose of 72 kDa and 74 kDa forms due to the heterogeneity of *N*-glycosylation (Otto et al., 1993; Garavito et al., 2002), only the smaller one was increased by the traumatic insults to the spinal cord. Using an immunohistochemical method, the spatial expression pattern of COX-2 protein induced in the spinal cord after traumatic SCI was investigated. Six hours after injury, COX-2 immunoreactivity was detected along the pia matters and blood vessels around the contused spinal cord (Fig. 2c and d), whereas no COX-2-positive cells were detected in any cells of the normal controls (Fig. 2e and f). Next, we performed double–immunofluorescence labeling to identify COX-2-positive cell types. COX-2-positive cells were positive for RECA-1, the marker protein of endothelial

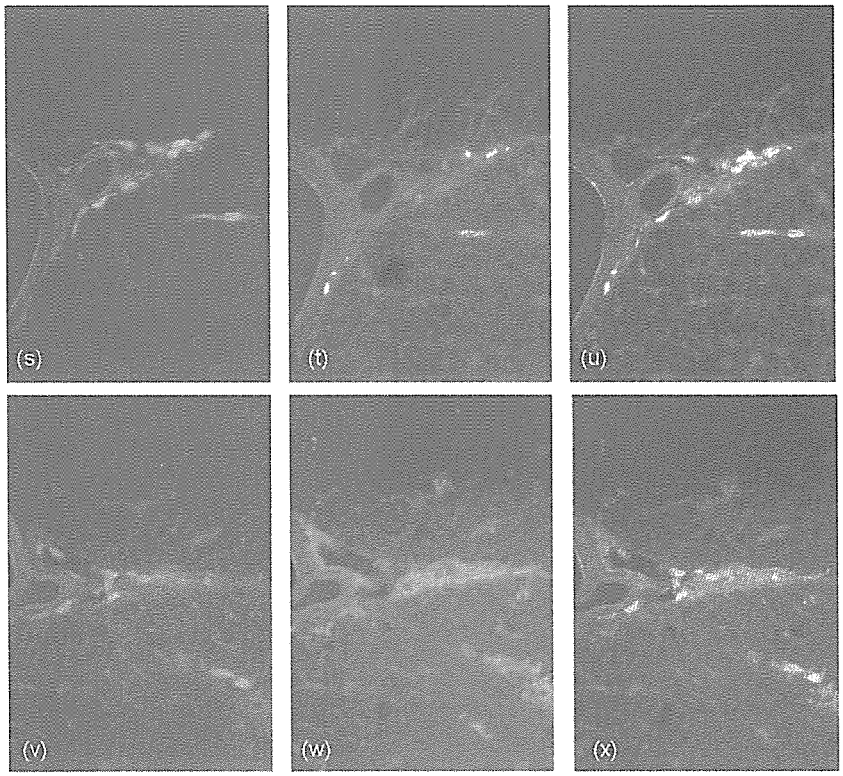

Fig. 3. (*Continued*).

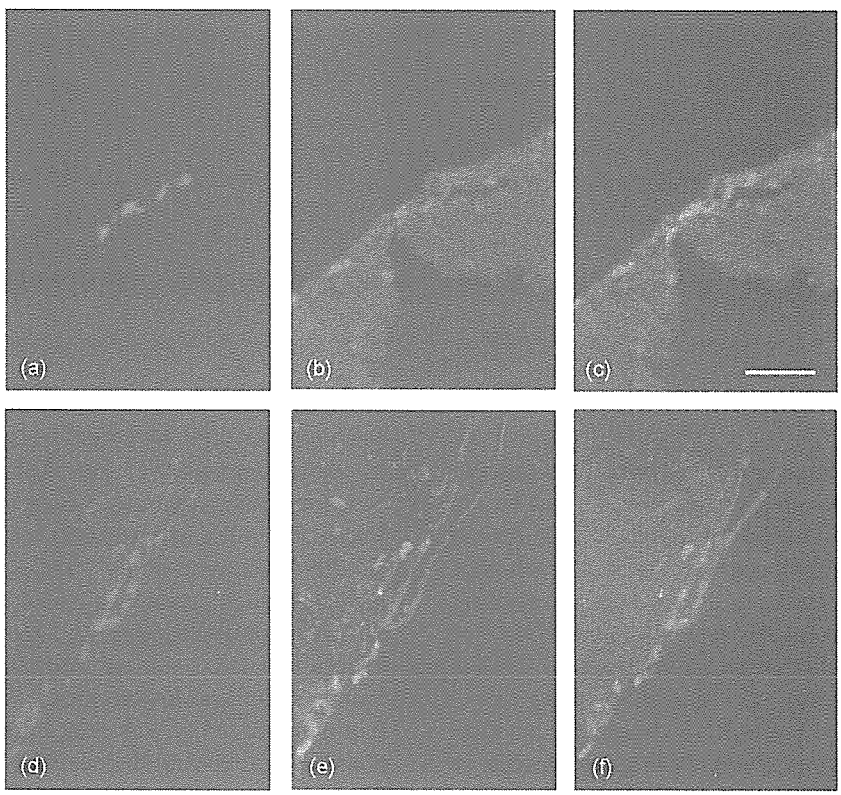

Fig. 4. Double-immunofluorescent staining of rat spinal cord injury, for COX-2 (red) and iNOS (green). COX-2 positive cells were visualized with Cy3-conjugated donkey antibody against mouse IgG as a secondary antibody (a and d). iNOS positive cells were visualized with FITC-conjugated donkey antibody against rabbit IgG as a secondary antibody (b and e). Superimposing the two-color images show that COX-2-positive cells were negative for iNOS and vice versa, and that there were some COX-2 positive cells nearby iNOS-positive cells (c and f). Scale bar = 50 μm. (For interpretation of the references to colour in this figure legend, the reader is referred to the web version of the article).

cells, in spinal cord 6 h after the injury (Fig. 3a–i). However, the COX-2 immunoreactivity in the spinal cord did not coincide with MAP2, GFAP, ED1, ED2, or OX42 expressed by neurons, astrocytes, monocytes, macrophages, or microglia, respectively, (Fig. 3j–x). Finally, we examined the spatial positional relation of COX-2 and iNOS after SCI. Six hours after injury, iNOS-positive cells appeared in intra-and perivascular zones, while some were scattered in the damaged area. There were some iNOS-positive cells standing nearby COX-2-positive cells (Fig. 4).

4. Discussion

We investigated the early stage temporal and spatial expression of *COX-2* gene after traumatic SCI. We found that *COX-2* gene was already induced at a half-maximal level 30 min after injury and COX-2 protein accumulation was observed in endothelial cells of blood vessels 6 h after injury. In cases of *COX-2* gene induction, Resnik reported that by using in situ hybridization COX-2 mRNA expression was detected in spinal cord neurons and around blood vessels at 2 h, 4 h, and 8 h following impaction (Resnick et al., 1998) and Tonai reported that by using Northern blotting COX-2 mRNA level was seen to increase 2 h after compression of the spinal cord (Tonai et al., 1999). In our experiment, *COX-2* gene induction after the injury was found to begin within 30 min; therefore, it seems that no new protein synthesis is required for its transcription. In addition, this immediate early expression in the spinal cord coincides well with those of iNOS (Satake et al., 2000a) and GDNF (Satake et al., 2000b). Therefore, it was postulated that the *COX-2* gene expressed in endothelial cells in addition to iNOS in macrophages and GDNF in microglia and macrophages seems to be induced by a common unidentified trigger that stimulates a pathway toward the NF-κB signaling. There are few reports of the localization of COX-2 after SCI (Resnick et al., 1998; Tonai et al., 1999), and none of them directly defined the types of cells or tissues where COX-2 protein was induced. Tonai reported that no clear expression of COX-2 was detected in any particular cell at 8 h after the injury, but instead showed that COX-2 protein was detected in polymorphonuclear leukocytes, glial cells, and vascular endothelial cells after intraparenchymal injection of 2 ng IL-1α, suggesting that induction of *COX-2* gene may be mediated by IL-1α (Tonai et al., 1999).

In this study, COX-2 protein induced after the acute injury was clarified to localize in endothelial cells using immunohistochemical double staining. However, we previously reported that iNOS-positive cells, macrophages and/or perivascular cells, appeared around the perivascular space at 6 h after traumatic SCI (Satake et al., 2000a). NO is known to cause the inflammation and the production of PGE_2 (Iyengar et al., 1987; Ialenti et al., 1992; Wong et al., 1996). In the present study, we observed that macrophages and endothelial cells co-existed along the pia matter and in blood vessels of the spinal cord 6 h after injury (Fig. 4). There are some reports on regulation of COX-2 activity and induction by NO using iNOS deficient mice (Guhring et al., 2000; Nogawa et al., 1998). Therefore, NO released by macrophage via iNOS seems to sustain high expression level of *COX-2* gene at least until 3 days after traumatic SCI since iNOS-positive cells were observed around the damaged area 2 days after the injury (Satake et al., 2000a). Further studies on the relationship of the mutual control between iNOS and COX-2 are required for development of better clinical treatments for patients who have suffered traumatic SCI.

5. Conclusion

COX-2 mRNA is induced within 30 min and COX-2 protein is increased in endothelial cells of blood vessels at 6 h following contusion injury of the spinal cord. *COX-2* gene induction after traumatic SCI seems not to require any new protein synthesis, and COX-2 protein accumulated in endothelial cells may be a component of the successive inflammatory processes in the damaged area.

References

Allen, A.R., 1914. Remarks on the histopathological changes in the spinal cord due to impact an experimental study. J. Nerv. Ment. Dis. 31, 141–147.

Breder, C.D., Saper, C.B., 1996. Expression of inducible cyclooxygenase mRNA in the mouse brain after systemic administration of bacterial lipopolysaccharide. Brain Res. 713, 64–69.

Chao, C.C., Lokensgard, J.R., Sheng, W.S., Hu, S., Peterson, P.K., 1997. IL-1-induced iNOS expression in human astrocytes via NF-κB. Neuroreport 8, 3163–3166.

DeWitt, D.L., 1991. Prostaglandin endoperoxide synthase: regulation of enzyme expression. Biochim. Biophys. Acta 1083, 121–134.

DeWitt, D.L., Smith, W.L., 1998. Primary structure of prostaglandin G/H synthase from sheep vesicular gland determined from the complementary DNA sequence. Proc. Natl. Acad. Sci. U.S.A. 85, 1412–1416.

Faden, A., 1993. Experimental neurobiology of central nervous system trauma. Crit. Rev. Neurobiol. 7, 175–186.

Fan, Z., Isobe, K., Kiuchi, K., Nakashima, I., 1995. Enhancement of nitric oxide production from activated macrophages by a purified form of ginsenoside (Rg1). Am. J. Chin. 23, 279–287.

Feng, L., Sun, W., Xia, Y., Tang, W., Chanmugam, P., Soyoola, E., Wilson, C.B., Hwang, D., 1993. Cloning two isoforms of rat cyclooxygenase: differential regulation of their expression. Arch. Biochem. Biophys. 307, 361–368.

Garavito, R.M., Malkowski, M.G., DeWitt, D.L., 2002. The structures of prostaglandin endoperoxide H synthases-1 and -2. Prostaglandins Other Lipid Mediat. 68–69, 129–152.

Guhring, H., Gorig, M., Mehmet, A., Coste, O., Zeilhofer, H.U., Pahl, A., Rehse, K., Brune, K., 2000. Suppressed injury-induced rise in spinal prostaglandin E2 production and reduced early thermal hyperalgesia in iNOS-deficient mice. J. Neurosci. 20, 6714–6720.

Ialenti, A., Ianaro, A., Moncada, S., Rosa, D.M., 1992. Modulation of acute inflammation by endogenous nitric oxide. Eur. J. Pharmacol. 211, 177–182.

Ichitani, Y., Shi, T., Haeggstrom, J.Z., Samuelsson, B., Hokfelt, T., 1997. Increased levels of cyclooxygenase-2 mRNA in the rat spinal cord after

peripheral inflammation: an in situ hybridization study. Neuroreport 8, 2949–2952.

Inoue, A., Ikoma, K., Morioka, N., Kumagai, K., Hashimoto, T., Hide, I., Nakata, Y., 1999. Interleukin-1 beta induces substance P release from primary afferent neurons through the cyclooxygenase-2 system. J. Neurochem. 73, 2206–2213.

Iyengar, R., Stuehr, D.J., Marletta, M.A., 1987. Macrophage synthesis of nitrite, nitrate, and N-nitrosamines: precursors and role of the respiratory burst. Proc. Natl. Acad. Sci. U.S.A. 84, 6369–6373.

Jobin, C., Morteau, O., Han, D.S., Sartor, R.B., 1998. Specific NF-κB blockade selectively inhibits tumour necrosis factor-α-induced COX-2 but not constitutive COX-1 gene expression in HT-29 cells. Immunology 95, 537–543.

Kujubu, D.A., Fletcher, B.S., Varnum, B.C., Lim, R.W., Herschman, H.R., 1991. TIS10, a phorbol ester tumor promoter-inducible mRNA from Swiss 3T3 cells, encodes a novel prostaglandin synthase/cyclooxygenase homologue. J. Biol. Chem. 266, 12866–12872.

Kujubu, D.A., Herschman, H.R., 1992. Dexamethasone inhibits mitogen induction of the TIS 10 prostaglandin synthase/cyclooxygenase gene. J. Biol. Chem. 267, 7991–7994.

Madrigal, J.L., Moro, M.A., Lizasoain, I., Lorenzo, P., Castrillo, A., Bosca, L., Leza, J.C., 2001. Inducible nitric oxide synthase expression in brain cortex after acute restraint stress is regulated by nuclear factor κB-mediated mechanisms. J. Neurochem. 76, 532–538.

Nakayama, M., Uchimura, K., Zhu, R.L., Nagayama, T., Rose, M.E., Stetler, R.A., Isakson, P.C., Chen, J., Graham, S.H., 1998. Cyclooxygenase-2 inhibition prevents delayed death of CA hippocampal neurons following global ischemia. Proc. Natl. Acad. Sci. U.S.A. 95, 10954–10959.

Nishiya, T., Uehara, T., Kaneko, M., Nomura, Y., 2000. Involvement of nuclear factor-κB (NF-κB) signaling in the expression of inducible nitric oxide synthase (iNOS) gene in rat C6 glioma cells. Biochem. Biophys. Res. Commun. 275, 268–273.

Nogawa, S., Forster, C., Zhang, F., Nagayama, M., Ross, M.E., Iadecola, C., 1998. Interaction between inducible nitric oxide synthase and cyclooxygenase-2 after cerebral ischemia. Proc. Natl. Acad. Sci. U.S.A. 95, 10966–10971.

O'Banion, M.K., Winn, V.D., Young, D.A., 1992. cDNA cloning and functional activity of a glucocorticoid-regulated inflammatory cyclooxygenase. Proc. Natl. Acad. Sci. U.S.A. 89, 4888–4892.

Otto, J.C., DeWitt, D.L., Smith, W.L., 1993. *N*-glycosylation of prostaglandin endoperoxide synthase-1 and -2 and their orientations in the endoplasmic reticulum. J. Biol. Chem. 268, 18234–18242.

Poligone, B., Baldwin, A.S., 2001. Positive and negative regulation of NF-κB by COX-2: roles of different prostaglandins. J. Biol. Chem. 276, 38658–38664.

Resnick, D.K., Graham, S.H., Dixon, C.E., Marion, D.W., 1998. Role of cyclooxygenase-2 in acute spinal cord injury. J. Neurotrauma. 15, 1005–1013.

Satake, K., Matsuyama, Y., Kamiya, M., Kawakami, H., Iwata, H., Adachi, K., Kiuchi, K., 2000a. Nitric oxide via macrophage iNOS induces apoptosis following traumatic spinal cord injury. Brain Res. Mol. Brain Res. 85, 114–122.

Satake, K., Matsuyama, Y., Kamiya, M., Kawakami, H., Iwata, H., Adachi, K., Kiuchi, K., 2000b. Up-regulation of glial cell line-derived neurotrophic factor (GDNF) following traumatic spinal cord injury. Neuroreport 11, 3877–3881.

Serou, M.J., DeCoster, M.A., Bazan, N.G., 1999. Interleukin-1 beta activates expression of cyclooxygenase-2 and inducible nitric oxide synthase in primary hippocampal neuronal culture: platelet-activating factor as a preferential mediator of cyclooxygenase-2 expression. J. Neurosci. Res. 58, 593–598.

Sirois, J., Levy, L.O., Simmons, D.L., 1993. Characterization and hormonal regulation of the promoter of the rat prostaglandin endoperoxide synthase 2 gene in granulosa cells. Identification of functional and protein-binding regions. J. Biol. Chem. 268, 12199–12206.

Smith, W.L., Garavito, R.M., DeWitt, D.L., 1996. Prostaglandin endoperoxide H synthases cyclooxygenases-1 and -2. J. Biol. Chem. 271, 33157–33160.

Tanaka, M., Ito, S., Kiuchi, K., 2000. Novel alternative promoters of mouse glial cell line-derived neurotrophic factor gene. Biochim. Biophys. Acta 1494, 63–74.

Tator, C.H., 1995. Update on the pathophysioloy and pathology of acute spinal cord injury. Brain Pathol. 5, 407–413.

Tator, C.H., Fehlings, M.G., 1991. Review of the secondary injury theory of acute spinal cord trauma with emphasis on vascular mechanisms. J. Neurosurg. 75, 15–26.

Tonai, T., Taketani, Y., Ueda, N., Nishisho, T., Ohmoto, Y., Sakata, Y., Muraguchi, M., Wada, K., Yamamoto, S., 1999. Possible involvement of interleukin-1 in cyclooxygenase-2 induction after spinal cord injury in rats. J. Neurochem. 72, 302–309.

Wong, M.L., Rettori, V., AL-Shekhlee, A., Bongiorno, P.B., Canteros, G., McCann, S.M., Gold, P.W., Licinio, J., 1996. Inducible nitric oxide synthase gene expression in the brain during systemic inflammation. Nat. Med. 2, 581–584.

Yamagata, K., Andreasson, K.I., Kaufmann, W.E., Barnes, C.A., Worley, P.F., 1993. Expression of a mitogen-inducible cyclooxygenase in brain neurons: regulation by synaptic activity and glucocorticoids. Neuron 11, 371–386.

Yamamoto, K., Arakawa, T., Ueda, N., Yamamoto, S., 1995. Transcriptional roles of nuclear factor kappa B and nuclear factor-interleukin-6 in the tumor necrosis factor alpha-dependent induction of cyclooxygenase-2 in MC3T3-E1 cells. J. Biol. Chem. 270, 31315–31320.

Available online at www.sciencedirect.com
SCIENCE DIRECT®
Virus Research 108 (2005) 23–28
Virus Research
www.elsevier.com/locate/virusres

A lentiviral expression system demonstrates that L* protein of Theiler's murine encephalomyelitis virus (TMEV) is essential for virus growth in a murine macrophage-like cell line

Toshiki Himeda[a], Yoshiro Ohara[a,*], Kunihiko Asakura[a], Yasuhide Kontani[a], Manabu Murakami[b], Hiromi Suzuki[c], Makoto Sawada[c]

[a] *Department of Microbiology, Kanazawa Medical University, 1-1 Uchinada, Ishikawa 920 0293, Japan*
[b] *Division of Basic Science, Medical Research Institute, Kanazawa Medical University, 1-1 Uchinada, Ishikawa 920 0293, Japan*
[c] *Institute for Comprehensive Medical Science, Fujita Health University, Aichi 470 1192, Japan*

Received 14 April 2004; received in revised form 14 July 2004; accepted 19 July 2004
Available online 17 September 2004

Abstract

The DA subgroup strains of Theiler's murine encephalomyelitis virus (TMEV) synthesize L* protein, which is translated out of frame with the polyprotein from an alternative AUG, 13 nucleotides downstream from the authentic polyprotein AUG. By a 'loss of function' experiment using a mutant virus, DAL*-1, in which the L* AUG is mutated to an ACG, L* protein is shown to play an important role in virus persistence, TMEV-induced demyelination, and virus growth in macrophages. In the present study, we established an L* protein-expressed macrophage-like cell line and confirmed the importance of L* protein in virus growth in this cell line.

Keywords: Theiler's murine encephalomyelitis virus; L* protein; Lentiviral vector; Virus growth; Macrophages

Theiler's murine encephalomyelitis virus (TMEV) belongs to the genus *Cardiovirus* of the family *Picornaviridae* and is divided into two subgroups (Ohara and Roos, 1987; Lipton and Jelachich, 1997; Obuchi and Ohara, 1998; Roos, 2002). DA (or TO) subgroup strains induce a non-fatal polioencephalomyelitis in weanling mice followed by virus persistence and chronic demyelination in the spinal cords. This late demyelinating disease serves as an experimental model of the human demyelinating disease, multiple sclerosis. In contrast, GDVII subgroup strains cause acute fatal polioencephalomyelitis without demyelination. The precise mechanisms of virus persistence and demyelination caused by DA subgroup strains are still unknown. A 17 kDa protein, called L*, is translated out of frame with the polyprotein from an alternative AUG, 13 nucleotides downstream from the authentic polyprotein AUG (Kong and Roos, 1991; Obuchi and Ohara, 1998; Roos, 2002). L* protein is only synthesized in the DA subgroup strains since the L* AUG is present in DA subgroup strains, but not in GDVII subgroup strains (Michiels et al., 1995; Obuchi and Ohara, 1998; Roos, 2002). Therefore, L* protein is thought to be a key protein regulating DA biological activities. A 'loss-of-function' experiment using a mutant virus, DAL*-1, in which the L* AUG initiation codon is mutated to an ACG, demonstrated that L* protein plays an important role in DA persistence and demyelination (Chen et al., 1995; Ghadge et al., 1998). However, that finding is still controversial since the absence of the L* AUG initiation codon in a different DA infectious clone had only a weak influence on the persistence of DA strain (van Eyll and Michiels, 2000, 2002).

We previously reported that DA strain grows in J774-1 cells, an *H-2*^{d} macrophage-like cell line derived from a tumor of a BALB/c mouse (Ralph et al., 1975), while the GDVII

* Corresponding author. Tel.: +81 76 218 8096; fax: +81 76 286 3961.
E-mail address: ohara@kanazawa-med.ac.jp (Y. Ohara).

0168-1702/$ – see front matter © 2004 Elsevier B.V. All rights reserved.
doi:10.1016/j.virusres.2004.07.009

strain does not (Obuchi et al., 1997). This phenomenon is of great interest since a major site for TMEV persistence is thought to be macrophages (Lipton and Jelachich, 1997; Obuchi and Ohara, 1998; Roos, 2002). The important role of L* protein in this in vitro phenomenon can be demonstrated by using DAL*-1 virus. DAL*-1 virus does not grow in murine monocyte/macrophage lineage cell lines, but it does grow in other cell lines, including neural cells (Obuchi et al., 1999). A recombinant virus, DANCL*/GD, which has the DA 5′ noncoding and L* protein coding regions replacing the corresponding regions of GDVII and therefore synthesizes L* protein, had a rescue of growth activity in J774-1 cells, suggesting that L* protein plays an important role in virus growth in macrophages (Obuchi et al., 2000).

A challenge in research related to L* protein is that its sequence overlaps with that of the polyprotein, making it impossible to introduce the DA L* coding sequence into the parental GDVII strain without changing the polyprotein sequence. The generation of macrophage cells that constitutively express L* protein would allow a confirmation of the role of this protein in virus growth with a 'gain of function' experiment. This system would also allow the synthesis of L* protein in the cytoplasm, as has been described (Obuchi et al., 2001), without being incorporated into virions. Therefore, the goal of the present study was to establish a macrophage cell line that constitutively expresses L* protein.

We used a lentiviral expression system in order to achieve a stable and efficient gene transfer of L* protein. The vector was constructed by using the transfer vector plasmid pCSII-EF-MCS-IRES-hrGFP, constructed by Dr. Hiroyuki Miyoshi and Dr. Tomoyuki Yamaguchi, Laboratory of Genetics, The Salk Institute for Biological Studies. The plasmid has sequences of a human elongation factor (EF) 1 α subunit gene promoter, a multiple cloning site (MCS), an internal ribosome entry site (IRES), and the coding region of a 'humanized, red-shifted' green fluorescent protein (hrGFP) in tandem. L* coding sequence was inserted into MCS, resulting in the production of L* protein independently from hrGFP and not as a fusion protein. The expression of both proteins is regulated by one promoter. Another construct, in which the 3xFLAG epitope sequence is tagged to the N-terminus of L* protein, was generated as an additional control since the 5′ one third of the L* protein coding region is important for its function (Obuchi et al., 2001). In order to generate vesicular stomatitis virus (VSV) G protein-pseudotyped lentiviral vector particles, the transfer vector plasmid pCSII-EF-(cDNA of L* or 3xFLAGL* protein)-IRES-hrGFP with the packaging plasmid pMDLg/pRRE, pRSV-Rev, and the VSV-G protein envelope plasmid pMD.G (Naldini et al., 1996) were tansfected into subconfluent 293T cells, a human embryonic kidney epithelial cell line expressing the simian virus 40 large T antigen, using a high-efficiency calcium-phosphate-mediated transfection method (Miyoshi et al., 1997; Miyoshi et al., 1998; Sambrook and Russell, 2001). High-titer virus stocks were prepared by centrifugation (43,600 × *g*, 3 h, 21 °C). The infectious titers were determined by counting the number of GFP-positive cells by fluorescence-activated cell sorting (FACS) analysis (FACSCalibur: BD Biosciences, San Jose, CA). J774-1 cells (2×10^5) were infected and transduced at a multiplicity of infection (M.O.I.) of 5. After the infection, the third subculture of L*-transduced and 3xFLAGL*-transduced J774-1 cells were seeded at a density of 0.5 cells per well onto 360 wells and 1200 wells of HLA plates (Greiner bio-one, Tokyo, Japan), respectively.

Cell propagation was observed in 27 wells of L*-transduced cells and 105 wells of 3xFLAGL*-transduced cells. During the first several passages, the cells in approximately 50% of wells were GFP-positive and propagated more slowly than the original J774-1 cells. Some showed a different morphology, such as enlargement (20–30 μm, about 1.5-fold larger in diameter) and an amoebic shape. We selected four L*-expressed (L*/J774) and eight 3xFLAGL*-expressed (3xFLAGL*/J774) clones by FACS analysis using expression of GFP. The cells formed clusters easily when replated in new culture dishes. These properties reverted to those of the original J774-1 cells after seven passages. When both cells were seeded in a 35 mm plastic culture dish at the density of 1×10^5 cells/ml, the cultures reached to the density of 1×10^6 cells/ml within about four days, with a doubling time of 24–30 h. Seven empty vector-transduced clones (control/J774) were also obtained from the empty vector-transduced J774-1 cells and served as a control. The properties of these cells were not different from those of the original J774-1 cells. Fig. 1 shows the histograms of L*/J774/6, 3xFLAGL*/J774/33 and control/J774/6 clones, which gave the highest GFP expression.

The expression of L* and 3xFLAGL* proteins was further confirmed by Western blotting using polyclonal rabbit anti-L* antibody (Ab) (Obuchi et al., 2000, 2001) or monoclonal mouse anti-FLAG M2 Ab (Sigma, St. Louis, MO). Enhanced chemiluminescence reagents, ECL plus (Amersham Biosciences, Buckinghamshire, UK), detected biotinylated secondary Ab and horseradish peroxidase-conjugated streptavidin (Fig. 2). The expression of L* or 3xFLAGL* protein was stable after forty passages of culture.

We examined and compared the growth kinetics of DAL*-1 virus in those cells. The culture supernatants and cell lysates of 1.5×10^6 cells infected with DAL*-1 virus at an M.O.I. of 10 PFU per cell were harvested at 0, 3, 6, 12, 24, and 48 h post-infection (p.i.), and the infectivity was assayed by a standard plaque assay on BHK-21 cells. In L*/J774/6 cells, the titers of cell-free and cell-associated DAL*-1 virus reached a peak at 12 h p.i. (6.3×10^5 and 3.8×10^5 PFU/ml, respectively) and then gradually decreased (Fig. 3B). On the other hand, the titers gradually decreased in control/J774/6 cells (Fig. 3A). The data indicated that L* protein is essential for DA growth in J774-1 cells. The titers of DAL*-1 virus also gradually decreased in 3xFLAGL*/J774/33 cells (Fig. 3C), suggesting that the N-terminus is important for the function of L* protein, as previously reported (Obuchi et al., 2001). In addition, even though the 3xFLAG epitope is a small peptide (2.7 kDa), it may have changed the higher-order structure of